



## Reversible Sigma C-C Bond Formation Between Phenanthroline Ligands Activated by (C<sub>5</sub>Me<sub>5</sub>)<sub>2</sub>Yb

Grégory A Nocton, Wayne A Lukens, Corwin A Booth, Sergio A Rozenel, Scott A Medling, Laurent Maron, Richard A Andersen

### ► To cite this version:

Grégory A Nocton, Wayne A Lukens, Corwin A Booth, Sergio A Rozenel, Scott A Medling, et al.. Reversible Sigma C-C Bond Formation Between Phenanthroline Ligands Activated by (C<sub>5</sub>Me<sub>5</sub>)<sub>2</sub>Yb. Journal of the American Chemical Society, 2014, 136 (24), pp.8626-8641. 10.1021/ja502271q . hal-01388838

**HAL Id: hal-01388838**

**<https://hal.science/hal-01388838>**

Submitted on 27 Oct 2016

**HAL** is a multi-disciplinary open access archive for the deposit and dissemination of scientific research documents, whether they are published or not. The documents may come from teaching and research institutions in France or abroad, or from public or private research centers.

L'archive ouverte pluridisciplinaire **HAL**, est destinée au dépôt et à la diffusion de documents scientifiques de niveau recherche, publiés ou non, émanant des établissements d'enseignement et de recherche français ou étrangers, des laboratoires publics ou privés.

# Reversible Sigma C-C Bond Formation Between Phenanthroline Ligands Activated by (C<sub>5</sub>Me<sub>5</sub>)<sub>2</sub>Yb

Grégory Nocton,<sup>\*†‡</sup> Wayne W. Lukens,<sup>§</sup> Corwin H. Booth,<sup>§</sup> Sergio S. Rozenel,<sup>‡§</sup> Scott A. Medling,<sup>§</sup> Laurent Maron,<sup>⊥</sup> and Richard A. Andersen<sup>\*‡,§</sup>

<sup>†</sup> Laboratoire de Chimie Moléculaire, CNRS, Ecole Polytechnique, Palaiseau, France.

<sup>‡</sup> Department of Chemistry, University of California, Berkeley, California, 94720, USA.

<sup>§</sup> Chemical Sciences Division, Lawrence Berkeley National Laboratory, Berkeley, California, 94720, USA.

<sup>⊥</sup> LPCNO, UMR 5215, Université de Toulouse-CNRS, INSA, UPS, Toulouse, France.

---

**Abstract.** The electronic structure and associated magnetic properties of the 1,10-phenanthroline adducts of Cp\*<sub>2</sub>Yb are dramatically different from those of the 2,2'-bipyridine adducts. The monomeric phenanthroline adducts are ground state triplets that are based upon trivalent Yb(III), f<sup>13</sup> and (phen<sup>-</sup>) that are only weakly exchange coupled, which is in contrast to the bipyridine adducts whose ground states are multiconfigurational, open-shell singlets in which ytterbium is intermediate valent (*J. Am. Chem. Soc.*, **2009**, *131*, 6480; *J. Am. Chem. Soc.*, **2010**, *132*, 17537). The origin of these different physical properties is traced to the number and symmetry of the LUMO and LUMO + 1 of the heterocyclic amine ligands. The bipy<sup>-</sup> has only one π\*<sub>1</sub> orbital of b<sub>1</sub> symmetry of accessible energy but phen<sup>-</sup> has two π\* orbitals of b<sub>1</sub> and a<sub>2</sub> symmetry that are energetically accessible. The carbon p<sub>x</sub>-orbitals have different nodal properties and coefficients and their energies and therefore populations change depending on the position and number of methyl substitutions on the ring. A chemical ramification of the change in electronic structure is that Cp\*<sub>2</sub>Yb(phen) is a dimer, when crystallized from toluene solution, but a monomer when sublimed at 180-190 °C. When 3,8-Me<sub>2</sub>phenanthroline is used, the adduct Cp\*<sub>2</sub>Yb(3,8-Me<sub>2</sub>phen) exist in the solution in a dimer-monomer equilibrium in which ΔG is near zero. The adducts with 3-Me, 4-Me, 5-Me, 3,8-Me<sub>2</sub> and 5,6-Me<sub>2</sub>-phenanthroline are isolated and characterized by solid state X-ray crystallography, magnetic susceptibility and L<sub>III</sub>-edge XANES spectroscopy as a function of temperature and variable temperature <sup>1</sup>H NMR spectroscopy.

---

## Introduction.

The concept of a ligand in a metal compound acting as a single-electron acceptor is a topic of much recent interest [eg. see “Forum” in volume 50 (issue 20) of *Inorganic Chemistry*]<sup>1</sup>. The accessibility of an empty orbital on a ligand in a coordination complex was originally referred to as a “non-innocent” ligand but this terminology does not clearly distinguish between metal-ligand back-bonding in which a pair of electrons is transferred to an empty orbital and metal-to-ligand charge transfer (MLCT) where a single electron is transferred to an empty ligand orbital. The latter process generates an electron-transfer complex in which an electron resides in the ligand LUMO, an electron hole remains on the metal-based orbital, and the ligand is referred to as a “redox active” ligand. The ground state electronic structure is then determined by how the biradical correlates the two electrons forming either a triplet state ( $S = 1$ ), in which the electrons are ferromagnetically coupled, or an open-shell singlet state ( $S = 0$ ), in which the electrons are antiferromagnetically coupled.

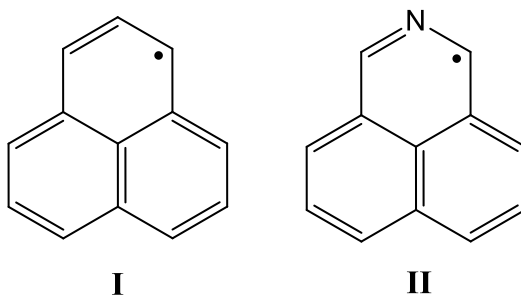
Complexes of d-transition metals with redox active ligands have been extensively and intensively studied.<sup>1</sup> In contrast, complexes of the f-block metals, although they are known, are not as well studied, with most of the work only appearing recently.<sup>2-14</sup> The 2,2'-bipyridine adducts of  $\text{Cp}^*_2\text{Yb}$ , in particular, have been shown by experimental and computational methodologies to have multiconfigurational open-shell singlet ground states in which ytterbium is intermediate valent.<sup>4,5</sup> In this context, an article by Scarborough and Wieghardt<sup>15</sup> is particularly informative as they systematize and classify the often confusing and/or contradictory literature of the 2,2'-bipyridine and related adducts of d-transition metal metallocenes using a density functional theory (DFT) broken-symmetry (BS) methodology. A comparison between the electronic ground state of  $(\text{C}_5\text{H}_5)_2\text{Ti}(\text{bipy})$ <sup>16</sup> and  $(\text{C}_5\text{Me}_5)_2\text{Yb}(\text{bipy})$  is enlightening. Both adducts have an open-shell singlet ground state (S)<sup>5,15</sup> but the triplet state (T) in  $\text{Cp}_2\text{Ti}(\text{bipy})$  lies close enough to the ground state ( $-2J = 600 \text{ cm}^{-1}$ ) that it is a spin

equilibrium molecule,  $S(M_S = 0) \rightleftharpoons T(M_S = 1)$ , whereas the triplet in  $\text{Cp}^*_2\text{Yb}(\text{bipy})$  lies 0.28 eV (calculated) or  $-2J = 0.11$  eV ( $920\text{ cm}^{-1}$ , experimental)<sup>11</sup> above the open-shell singlet state and the triplet is not significantly populated at 300 K. These physical properties show that strong exchange coupling does indeed occur in these 4f-block metal compounds.

Although bipyridine and related ligands, such as diazadienes, attached to d- and f-block metallocenes have attracted the most attention, adducts with 1,10-phenanthroline have been largely ignored. Previous studies of  $\text{Cp}^*_2\text{Yb}(\text{phen})$  show that  $\text{Cp}^*_2\text{Yb}(\text{phen})$  and  $\text{Cp}^*_2\text{Yb}(\text{bipy})$  are analogous in many respects.<sup>6,14</sup> In particular the electrochemistry of the two complexes is almost identical.<sup>6</sup> In this article, it is shown that the ground state of  $\text{Cp}^*_2\text{Yb}(\text{phen})$  is a triplet (T), in contrast to the open-shell singlet ground state of  $\text{Cp}^*_2\text{Yb}(\text{bipy})$ . One chemical ramification of the triplet electronic configuration is that the phenanthroline ligands in the individual monomer units are coupled by formation of a C-C sigma bond at the 4,4'-positions resulting in a dimer. The related adduct,  $\text{Cp}^*_2\text{Yb}(3,8\text{-Me}_2\text{-phen})$  exists in solution as a dimer  $\rightleftharpoons$  monomer equilibrium, and analysis of solid state structure and  $^1\text{H}$  NMR spectra show that C-C bond is long ( $1.592(16)\text{ \AA}$ ) and weak ( $\Delta H = -8\text{ kcal.mol}^{-1}$ ).

The thermochemistry for a dimer  $\rightleftharpoons$  monomer equilibrium,  $D \rightleftharpoons 2M$ , where M is an organic  $\sigma$ -radical,  $\sigma\text{-R}$ , and D is the dimer,  $\sigma\text{-R}_2$ , is of fundamental interest since the value of  $\Delta H$  is the bond dissociation enthalpy, BDE, for the  $\sigma\text{-R}_2$  single bond. Although BDE's for organic compounds are well known, only a few examples of BDE's for a specific  $\sigma$ -carbon-carbon single bond and the associated bond distance in the dimer are known. The oldest dimer-monomer equilibrium is that of Gomberg's dimer, for which the value of  $\Delta H$  of  $11\text{ kcal.mol}^{-1}$  has been measured,<sup>17-19</sup> is not a simple  $\sigma\text{-R}_2 \rightleftharpoons 2\sigma\text{-R}$  dissociation due to the structure of the dimer. Recently, the thermochemistry of the  $\sigma$ -dimerization of the phenalenyl

$\sigma$ -dimer and the related aza-analogue have been measured.<sup>20-22</sup> The  $\Delta H$  values of  $D \rightleftharpoons 2M$  for **I** and **II** in  $\text{CCl}_4$  are  $10 \text{ kcal.mol}^{-1}$  and  $11 \text{ kcal.mol}^{-1}$ , respectively, and the associated  $\Delta S$  values are  $15$  and  $18 \text{ cal.mol}^{-1}.\text{K}^{-1}$  respectively. The C-C bond length in the copper bis(trifluoroacetetylacetonate) complex of the dimer of **II** is  $1.58 \text{ \AA}$ . This value is identical to that calculated for the  $\sigma$ -C-C distance in the  $\sigma$ -dimer of **I**, for which the calculated value of the BDE is  $16 \text{ kcal.mol}^{-1}$ . More recently, the  $\Delta H$  value for the  $D \rightleftharpoons 2M$ , M is 2,6-di-tert-butyl-4-methoxyphenoxy radical of  $6 \text{ kcal.mol}^{-1}$  has been obtained along with the  $\sigma$ -C-C distance in the dimer of  $1.605(2) \text{ \AA}$ .<sup>23</sup> The reversible coupling of two pyridine ligands in a  $\beta$ -diketiminate iron complex has recently been published in which the C-C distance of  $1.563(6) \text{ \AA}$  was measured and a  $\Delta H$  value of  $11 \text{ kcal.mol}^{-1}$  was estimated.<sup>24</sup>

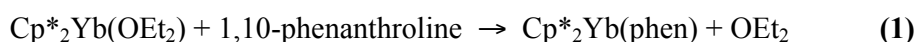


The dimer of the phenalenyl radical also forms  $\pi$ -dimers when  $\text{Me}_3\text{C}$  groups are attached to the arene rings.<sup>25-27</sup> Although the  $\Delta H$  values are similar to the  $\sigma$ -dimers, the  $\pi$ -C-C distances are much longer, as they range from  $3.201(8) \text{ \AA}$  to  $3.323(6) \text{ \AA}$  in the  $\pi$ -dimer of 1,4,7- $(\text{Me}_3\text{C})_3\text{C}_{12}\text{H}_6$  in  $D_{3d}$  symmetry.

This article shows that single electron transfer (SET) to a  $\pi$ -symmetry LUMO of a close-shell ligand results in a stretched and weakened C-C bonds,  $\sigma\text{-R}_2$  for which  $\Delta G \sim 0$ .

## Results.

**Synthesis.** The syntheses of  $\text{Cp}^*_2\text{Yb}(\text{phen})$  and  $[\text{Cp}^*_2\text{Yb}(\text{phen})]\text{I}$  were reported in an earlier paper,<sup>14</sup> and the new neutral adducts are prepared in a similar manner, Eq. 1. Some physical properties of the adducts are shown in Table 1.

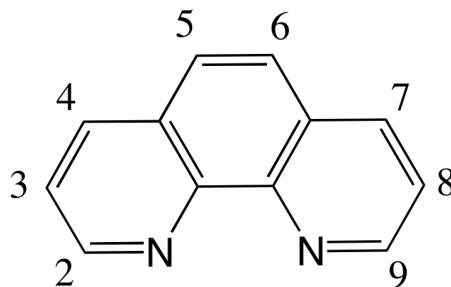


The neutral phen adducts of  $\text{Cp}^*_2\text{Yb}$ ,  $\text{Cp}^*_2\text{Yb}(\text{x-phen})$ , where x is H, 3-Me, 4-Me and 5-Me (The atom numbering system is shown in the legend to Table 1) are sparingly soluble in toluene and tetrahydrofuran, they decompose in dichloromethane, and may be crystallized from a dilute solution of warm toluene. The 3,8-Me<sub>2</sub>phen adduct is somewhat more soluble in toluene, but all of the neutral adducts are much less soluble than the 2,2'-bipyridine adducts described in earlier papers.<sup>4,5,14,28</sup> The solid-state and solution-state physical properties of the adducts are quite different and these properties are described in the separate sections that follow. The neutral phen adduct may also be sublimed at 190 °C under reduced pressure to yield dark purple crystalline material. The products of the crystallization and sublimation of  $\text{Cp}^*_2\text{Yb}(\text{phen})$ , **1**, are referred as **1-crystallized** and **1-sublimed** in Table 1

**Table 1.** Solid state properties of the  $\text{Cp}^*_2\text{Yb}$  adducts **1-7**. The legend shows the numbering scheme for the carbon positions on phenanthroline.

Compound	color	m.p (°C)	IR (cm <sup>-1</sup> )	$\mu_{\text{eff}}$ (300K) <sup>(a)</sup>
$\text{Cp}^*_2\text{Yb}(\text{phen})$ ( <b>1-crystallized</b> )	deep blue	297-300	1610, 1590, 1550, 859	4.00
$\text{Cp}^*_2\text{Yb}(\text{phen})$ ( <b>1-sublimed</b> )	deep blue	297-300	1610, 1590, 1550, 859	4.35
$[\text{Cp}^*_2\text{Yb}(\text{phen})]^+\text{I}^-$ ( <b>2</b> )	red-brown	175-180	1622, 1518, 855	4.54
$\text{Cp}^*_2\text{Yb}(3,8\text{-Me}_2\text{phen})$ ( <b>3</b> )	dark red	286-288	1625, 1573, 1461, 799	4.10
$\text{Cp}^*_2\text{Yb}(3\text{-Mephen})$ ( <b>4</b> )	dark purple	270-272	1612, 1554, 880	3.92
$\text{Cp}^*_2\text{Yb}(4\text{-Mephen})$ ( <b>5</b> )	dark purple	254-256	1618, 1512, 1445, 800	3.92
$\text{Cp}^*_2\text{Yb}(5\text{-Mephen})$ ( <b>6</b> )	dark purple	280-283	1626, 1578, 1504, 878	3.95
$\text{Cp}^*_2\text{Yb}(5,6\text{-Me}_2\text{phen})$ ( <b>7</b> )	deep purple	285-287	1605, 1584, 1480, 804	3.68

a) the magnetic moments correspond to the formulation given in the first column.



### Physical Properties, Solid State.

#### Magnetism.

Plots of the effective magnetic moment per Yb,  $\mu_{\text{eff}}$ , as a function of temperature for the six neutral adducts **1-crystallized**, **1-sublimed** and **3-7**, each obtained by crystallization from toluene and the cation  $[\text{Cp}^*_2\text{Yb}(\text{phen})]^+\text{I}^-$  (**2**), are shown in Figures 1 and 2 (Plots of  $\chi$ ,  $\chi T$ ,  $1/\chi$  and  $\chi T$  as a function of temperature are available in SI) and  $\mu_{\text{eff}}$  are reported in Table 1. The striking feature of the data in Figures 1 and 2 is that the curves have a similar shape that differ mainly by a scaling factor for the neutral and cationic adducts, although the overall magnitude of the  $\mu_{\text{eff}}$  value for **7** is noticeably smaller over the entire temperature range. This similarity is in contrast to what was observed for the various bipyridine adducts of  $\text{Cp}^*_2\text{Yb}$  described in earlier work in which the neutral bipy adducts have substantially lower  $\mu_{\text{eff}}$  values relative to their cationic derivatives.<sup>4,5,28</sup>

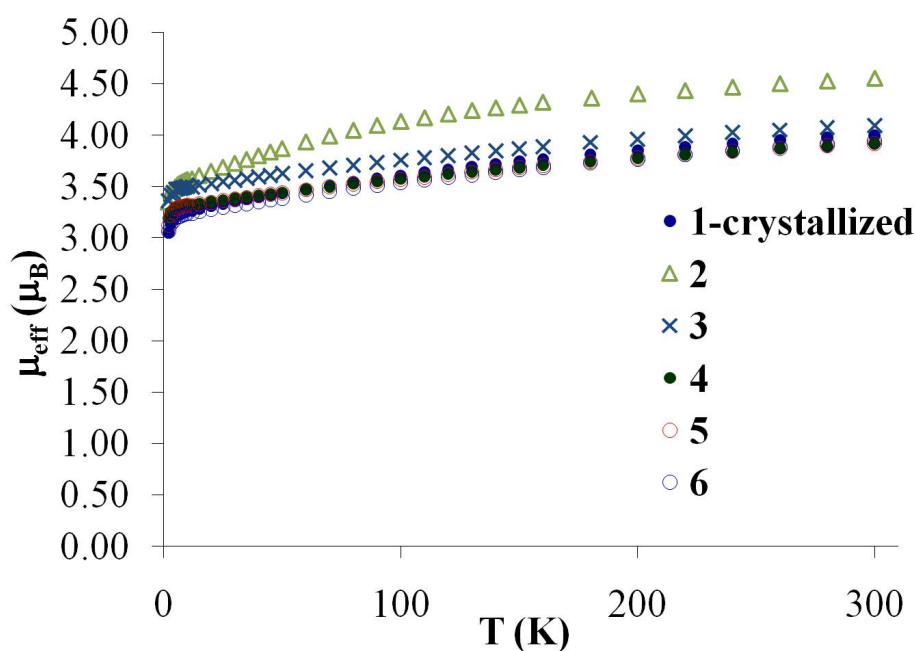


**Figure 1.** Plot of the effective magnetic moment,  $\mu_{\text{eff}}$  per Yb, as a function of temperature for **1-6** in the 2-300 K temperature range. These adducts are obtained by crystallization.

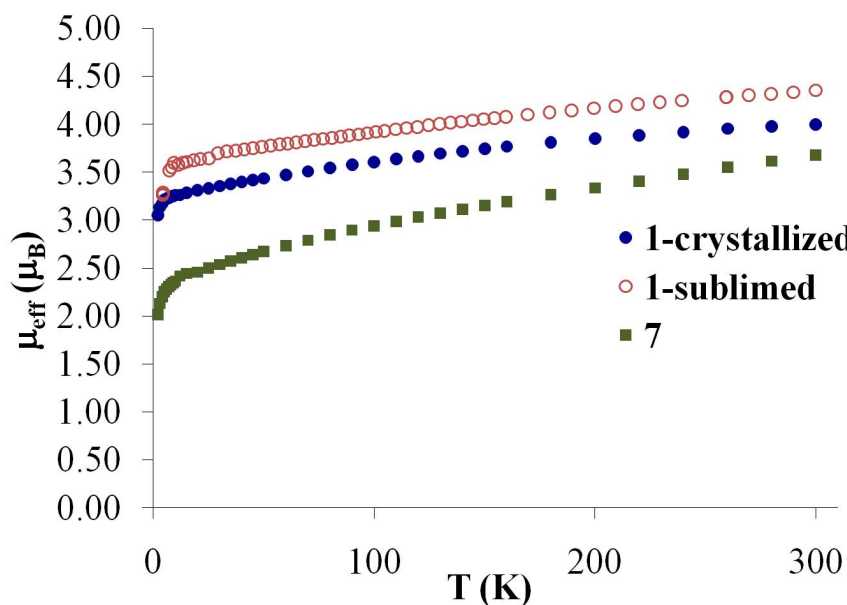


**Figure 2.** Plot of the effective magnetic moment,  $\mu_{\text{eff}}$  per Yb, as a function of temperature for **1-monomer** after sublimation (red unfilled dots), see Figure 5, **1-dimer** after crystallization (blue filled dots), see Figure 8, and **7** after crystallization (green squares), see Figure 7, in the 2-300 K temperature range.

The effective magnetic moments of most of the neutral adducts have a slight temperature dependence as  $\mu_{\text{eff}}$  decreases from about 4  $\mu_B$  to 3.2  $\mu_B$  as the temperature decreases from 300



K to 5 K. The value of  $\mu_{\text{eff}}$  is somewhat lower than expected for two uncorrelated spin carriers Yb(III),  $^2F_{7/2}$ , and phen radical anion,  $^2S_{1/2}$ , for which a value of  $4.83 \mu_B$  is expected at 300 K. The value of  $4.54 \mu_B$  is expected for an isolated Yb(III) ion,  $^2F_{7/2}$ , in agreement with the value found for the cationic adduct,  $[\text{Cp}^*_2\text{Yb}(\text{phen})]^+\text{I}^-$  (**2**), at 300 K. The similarity of the magnetic moments of the neutral adducts in Figures 1 and 2 with that of the cation begets the question of the identity of the anion in these neutral adducts. This question is amplified by the difference between the room temperature magnetic moment of sublimed, **1-sublimed**,  $4.5 \mu_B$ , and that of the recrystallized, complex, **1-crystallized**  $4.0 \mu_B$ . Although it has similar magnetic behavior,  $\mu_{\text{eff}}$  of **7** decreases from  $3.5 \mu_B$  to below  $2.5 \mu_B$  as the temperature decreases from 300 K to 5 K.

#### Yb L<sub>III</sub>-Edge XANES Spectra.

Yb L<sub>III</sub>-edge XANES spectra of the six neutral adducts, **1-crystallized** and **3-7**, are shown in Figure 3 for data collected at both 30 K and 300 K. No significant change is observed over this temperature range. All the spectra are characterized by a single white-line feature at about 8946 eV. This feature is indicative of the  $f^{13}$  configuration. Another peak at 8939 eV, indicating the  $f^{14}$  configuration as shown in Figure 3 by data on the intermediate valent  $\text{Cp}^*_2\text{Yb}(4\text{-Me-bipy})$  compound,<sup>4</sup> **8**, is not clearly visible in the phen adduct spectra. These spectra were fit with methods described previously,<sup>5</sup> giving estimates of  $n_f$  as shown in Table 2. The Yb in these samples is found to be close to trivalent, Yb(III), with an f-hole occupancy  $n_f \approx 1$ .

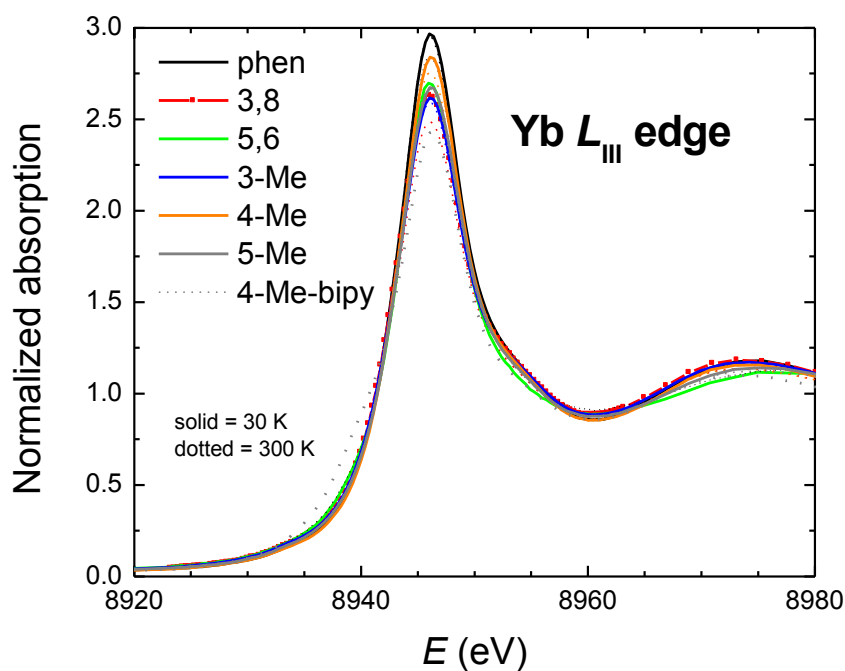


**Figure 3.** Yb  $L_{III}$ -edge XANES spectra for **1-crystallized** and **3-7** at 30 K (solid) and at 300 K (dotted). Also shown are previous data<sup>4</sup> on  $Cp^*_2Yb(4-Me-bipy)$  ( $n_f = 0.79$ ) for comparison. The shoulder at 8939 eV below the main peak at 8946 eV is indicative of the Yb(II) contribution, which is clearly seen in the bipy adduct data. The strong overlap of all the measured phen adduct data emphasizes the overall similarity in f-orbital occupancy. The small shoulder for each of the phen adducts indicates these samples are close to trivalent Yb.

**Table 2:** The estimated f-hole occupancy,  $n_f$ , determined by Yb L<sub>III</sub>-edge XANES measurements. No temperature dependence was observed between 30 K and 300 K. The estimated absolute error in the last digit  $n_f$  is shown in parentheses; the random error between separate traces is much smaller.

Compound	$n_f$
Cp* <sub>2</sub> Yb(phen) ( <b>1-crystallized</b> )	0.99(3)
Cp* <sub>2</sub> Yb(3,8-Me <sub>2</sub> phen) ( <b>3</b> )	0.96(3)
Cp* <sub>2</sub> Yb(3-Mephen) ( <b>4</b> )	0.95(3)
Cp* <sub>2</sub> Yb(4-Mephen) ( <b>5</b> )	0.98(3)
Cp* <sub>2</sub> Yb(5-Mephen) ( <b>6</b> )	0.97(3)
Cp* <sub>2</sub> Yb(5,6-Me <sub>2</sub> phen) ( <b>7</b> )	0.96(3)
Cp* <sub>2</sub> Yb(4-Me-bipy) ( <b>8</b> )	0.79 <sup>4</sup>

It is clear from Figure 3 that the Cp\*<sub>2</sub>Yb fragments are based upon Yb(III),  $f^{13}$ , which again begets the question raised from the magnetic data about the identity of the anion in the neutral adducts. The genesis of an answer is indicated by the EPR spectra.

### EPR Spectra.

The EPR Spectra at 2 K of Cp\*<sub>2</sub>Yb(phen) (**1-crystallized**) and Cp\*<sub>2</sub>Yb(3,8-Me<sub>2</sub>phen) (**3**) are shown in Figure 4(a) and that of [Cp\*<sub>2</sub>Yb(phen)]I (**2**) is shown in Figure 4(b). EPR spectra of the monomethyl adducts of Cp\*<sub>2</sub>Yb, **4-6** are shown in Supporting Information. The g-values are given in Table 3. Because of the high sensitivity of EPR, it is important to compare the EPR and magnetic susceptibility results to determine whether they are consistent. At the temperature at which the EPR spectra are obtained (~2 K), only the ground state is occupied in most cases. The effective magnetic moment of the ground state is determined from the EPR g-values using  $\mu_{\text{eff}} = 0.5 (g_1^2 + g_2^2 + g_3^2)^{1/2}$ , which may be compared to the magnetic susceptibility data by extrapolating  $\chi T$  to 0 K then determining  $\mu_{\text{eff}}(0 \text{ K})$ . As shown in Table 3, the effective magnetic moments determined from the EPR g-values are consistent with

those determined by magnetic susceptibility, so the EPR spectra can be assigned to the Yb complexes rather than to impurities.

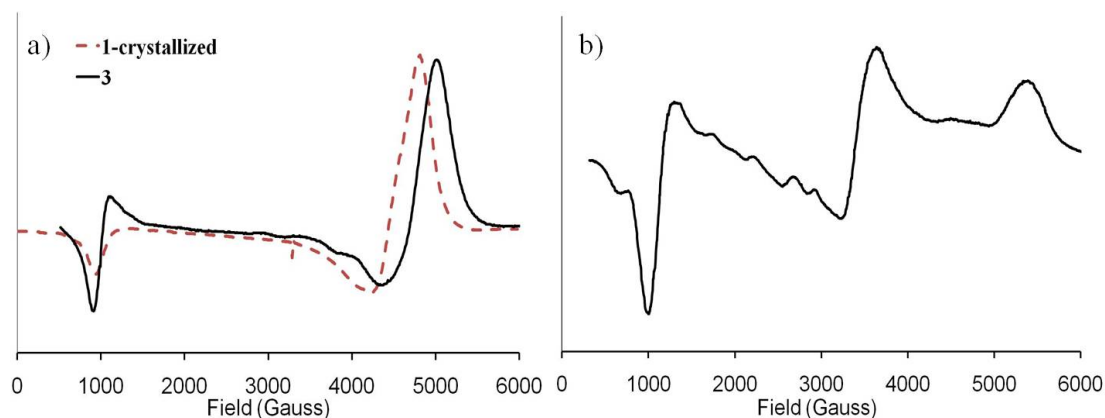


**Figure 4:** EPR spectra recorded in the solid state (powder) at 2 K for a)  $\text{Cp}^*_2\text{Yb}(\text{phen})$  (**1-crystallized**, solid black line) and  $\text{Cp}^*_2\text{Yb}(3,8\text{-Me}_2\text{phen})$  (**3**, dashed red line) and b)  $[\text{Cp}^*_2\text{Yb}(\text{phen})]\text{I}$  (**2**).

The EPR spectrum of **2** constitutes of a highly anisotropic rhombic signal that is awaited for a Yb(III) signal. Complexes **1-crystallized** and **3** also show a very similar anisotropic rhombic signal. The nature of the ligand coordinated to the  $[\text{Cp}^*_2\text{Yb}]^+$  fragment has a significant effect on the EPR spectrum as previously illustrated by  $[\text{Cp}^*_2\text{Yb}(\text{bipy})]\text{I}$  and  $\text{Cp}^*_2\text{Yb}(\text{bipy})$ .<sup>29</sup> In  $[\text{Cp}^*_2\text{Yb}(\text{bipy})]\text{I}$ ,  $[\text{Cp}^*_2\text{Yb}]^+$  is coordinated by a neutral, closed-shell bipy ligand, and the complex has EPR parameters similar to those of **2**. On the other hand, in  $\text{Cp}^*_2\text{Yb}(\text{bipy})$ ,  $[\text{Cp}^*_2\text{Yb}]^+$  is coordinated by the bipy radical anion, and  $\text{Cp}^*_2\text{Yb}(\text{bipy})$  is EPR silent. This was attributed to the consequence of the correlation of the two radicals (the hole of the Ytterbium center and the bipy radical anion) within this molecule. The lack of an EPR spectrum for **7** is consistent with the presence of the ligand that is a radical anion that correlates somehow with the ytterbium center. In contrast to this, the EPR spectra of **1-crystallized-6** are consistent with trivalent,  $[\text{Cp}^*_2\text{Yb}]^+$  fragments coordinated by closed-shell ligands. The fact that  $[\text{Cp}^*_2\text{Yb}(\text{phen})]\text{I}$  (**2**), is EPR active is unsurprising – the  $[\text{Cp}^*_2\text{Yb}]^+$  fragment is obviously

coordinated by a neutral phenanthroline ligand, and the charge is balanced by iodide. However, the fact that **1-crystallized** and **3-6** are EPR-active is surprising since it means that these complexes do not contain radical anions in sharp contrast to  $\text{Cp}^*\text{Yb}(\text{bipy})$ . Like the magnetic susceptibility data, the EPR results call into question the identity of the anion, *viz.* the electronic structure of the phenanthroline, in these neutral adducts.

**Table 3.** EPR data for **1-crystallized-7**.

	EPR data	$\mu_{\text{eff}}(\text{EPR})^{\text{a}}$	$\mu_{\text{eff}}(0 \text{ K})^{\text{b}}$
$\text{Cp}^*\text{Yb}(\text{phen})$ ( <b>1-crystallized</b> )	$g_1 = 6.85, g_2 = 1.47, g_3 = 1.40$	$3.57 \mu_{\text{B}}$	$3.21 \mu_{\text{B}}$
$[\text{Cp}^*\text{Yb}(\text{phen})]^+\text{I}^-$ ( <b>2</b> )	$g_1 = 6.70, g_2 = 1.92, g_3 = 1.21$	$3.54 \mu_{\text{B}}$	$3.49 \mu_{\text{B}}$
$\text{Cp}^*\text{Yb}(3,8\text{-Me}_2\text{phen})$ ( <b>3</b> )	$g_1 = 7.01, g_2 = 1.41, g_3 = 1.33$	$3.64 \mu_{\text{B}}$	$3.46 \mu_{\text{B}}$
$\text{Cp}^*\text{Yb}(3\text{-Mephen})$ ( <b>4</b> )	$g_1 = 7.02, g_2 = 1.21, g_3 = 1.21$	$3.61 \mu_{\text{B}}$	$3.29 \mu_{\text{B}}$
$\text{Cp}^*\text{Yb}(4\text{-Mephen})$ ( <b>5</b> )	$g_1 = 6.47, g_2 = 1.31, g_3 = 1.31$	$3.37 \mu_{\text{B}}$	$3.28 \mu_{\text{B}}$
$\text{Cp}^*\text{Yb}(5\text{-Mephen})$ ( <b>6</b> )	$g_1 = 6.45, g_2 = 1.42, g_3 = 1.21$	$3.35 \mu_{\text{B}}$	$3.19 \mu_{\text{B}}$
$\text{Cp}^*\text{Yb}(5,6\text{-Me}_2\text{phen})$ ( <b>7</b> )	EPR silent	-	$2.33 \mu_{\text{B}}$

a)  $\mu_{\text{eff}}(\text{EPR}) = (1/2)(g_1^2 + g_2^2 + g_3^2)^{1/2}$

b)  $\mu_{\text{eff}}(0 \text{ K})$  was determined by using a linear fit of  $\chi T$  from 12 K to 45 K, and determining  $\mu_{\text{eff}}$  from  $\chi T$  extrapolated to 0 K.

### X-Ray Crystal Structures.

The nature of the bonding in these complexes and the reason why **1-crystallized** and **3-6** are EPR active, in contrast to **7**, is clarified by their crystal structures. Although the phen adduct and substituted phen adducts are sparingly soluble in hydrocarbons and they have high melting points, Table 1, the phen adduct sublimates at 180 – 190 °C in an ampoule sealed under reduced pressure. The sublimation temperature must be maintained in this 10 °C range, since heating to a higher temperature results in substantial decomposition. In the 180 – 190 °C range, a small number of well formed crystals grow during one week, which are suitable for X-ray diffraction. The ORTEP in Figure 5 shows that the sublimed crystals are well separated monomers of  $\text{Cp}^*\text{Yb}(\text{phen})$  (**1-monomer** is now used to distinguish the sublimed compound

from the crystallized compound, labeled as **1-dimer**). The ORTEP of  $\text{Cp}_2^*\text{Yb}(\text{5,6-Me}_2\text{phen})$  (**7**) in Figure 6 shows the three independent molecules in the unit cell of the monomeric adduct obtained by crystallization from cyclohexane. The crystal structure of  $\text{Cp}^*_2\text{Yb}(\text{5,6-Me}_2\text{phen})$ , obtained by sublimation in a sealed ampoule under reduced pressure at 195 °C over two months, labeled **7-sublimed** is shown in Figure 7a, along with a crystal packing diagram of two molecules in the unit cell is shown in Figure 7b. These results contrast with the X-ray crystals structures of crystallized  $\text{Cp}^*\text{Yb}(\text{phen})$  (**1-dimer, crystallized**) and  $\text{Cp}^*\text{Yb}(\text{3,8-Me}_2\text{phen})$  (**3**), which are dimers. Crystals of the latter two compounds, obtained from toluene solution are deep blue and deep purple in color, respectively. ORTEP's of **1-dimer** and **3** are shown in Figure 8 and Figure 9, respectively. It is clear that the anionic partner is derived by dimerization of two phenanthroline radical anions by formation of a C-C bond at the 4,4'-positions, forming the diamagnetic dianionic partner. Similar, reductively driven bond formation between f-metal complexes is observed in uranium Schiff base complexes in which C-C bonds are formed upon reduction.<sup>30,31</sup>

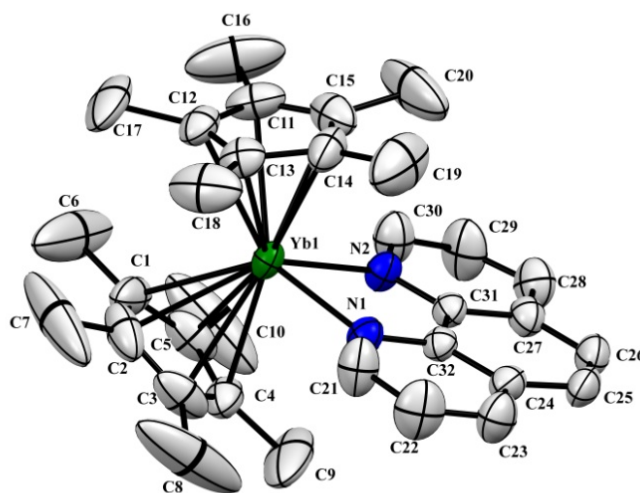


**Figure 5:** ORTEP for sublimed  $\text{Cp}^*_2\text{Yb}(\text{phen})$  (**1-monomer, sublimed**) (thermal ellipsoids at 50% level). Ytterbium atom is in green, nitrogen atoms in blue and carbon atoms in grey. All non-hydrogen atoms are refined anisotropically and the hydrogen atoms are placed in calculated positions but not refined. Hydrogen atoms have been omitted for clarity.

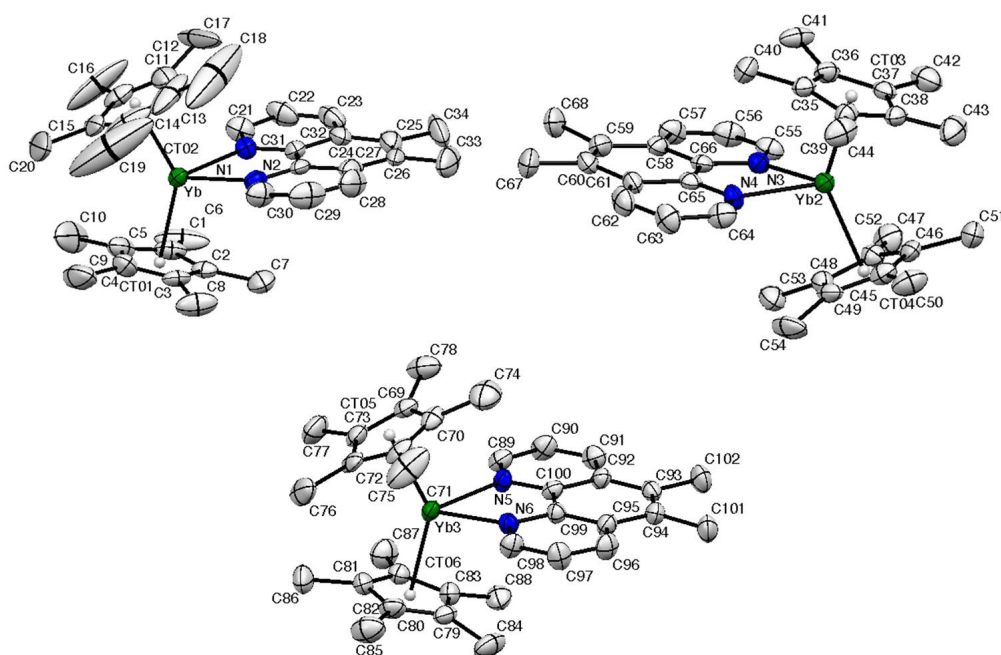


**Figure 6:** ORTEP for crystallized  $\text{Cp}^*_2\text{Yb}(5,6\text{-Me}_2\text{phen})$  (**7-crystallized**) (thermal ellipsoids at 50% level) showing the three independent molecules in the unit cell. Ytterbium atom is in green, nitrogen atoms in blue and carbon atoms in grey. All non-hydrogen atoms are refined anisotropically and the hydrogen atoms are placed in calculated positions but not refined. Hydrogen atoms have been omitted for clarity.

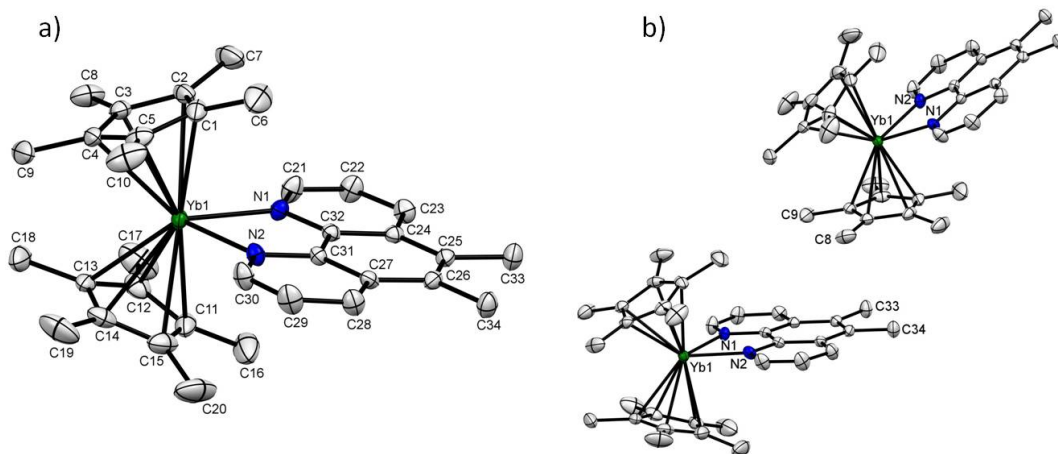


**Figure 7.** (a) ORTEP for crystallized  $\text{Cp}^*_2\text{Yb}(5,6\text{-Me}_2\text{phen})$  (**7-sublimed**) (thermal ellipsoids at 50% level). Ytterbium atom is in green, nitrogen atoms in blue and carbon atoms in grey. All non-hydrogen atoms are refined anisotropically and the hydrogen atoms are placed in calculated positions and refined isotropically. Hydrogen atoms have been omitted for clarity. (b) A portion of the packing diagram showing two molecules in the unit cell, showing the shortest C...C contact distances are between C(8) and C(9) methyl groups on the  $\text{Cp}^*$ -ring and C(34) and C(35) methyl groups on the 5,6- $\text{Me}_2\text{phen}$  ligand of 3.634 Å and 3.792 Å, respectively.

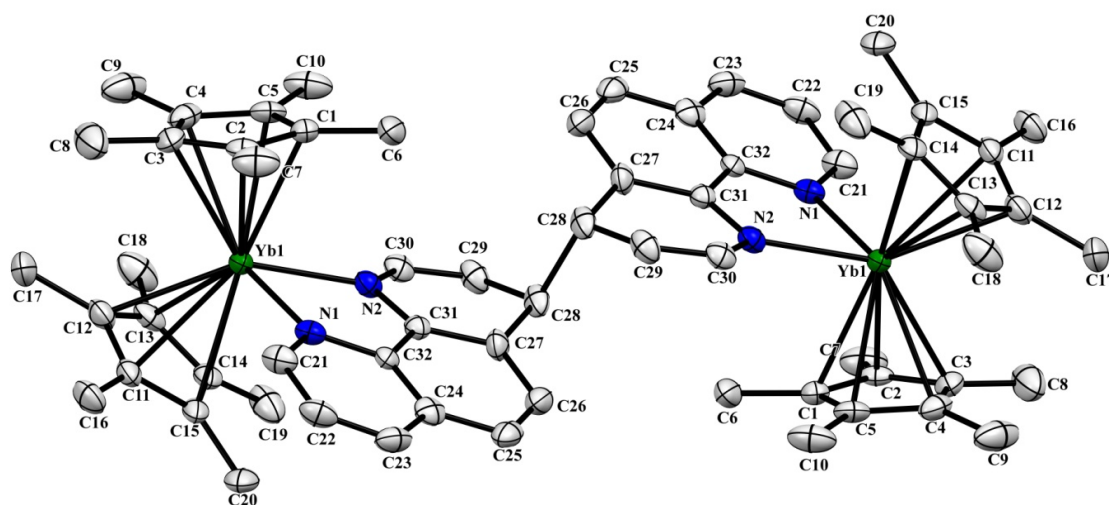


**Figure 8:** ORTEP for crystallized  $\text{Cp}^*_2\text{Yb}(\text{phen})$  (**1-dimer, crystallized**) (thermal ellipsoids at 50% level). All non-hydrogen atoms are refined anisotropically and the hydrogen atoms are placed in calculated positions but not refined. Hydrogen atoms have been omitted for clarity.

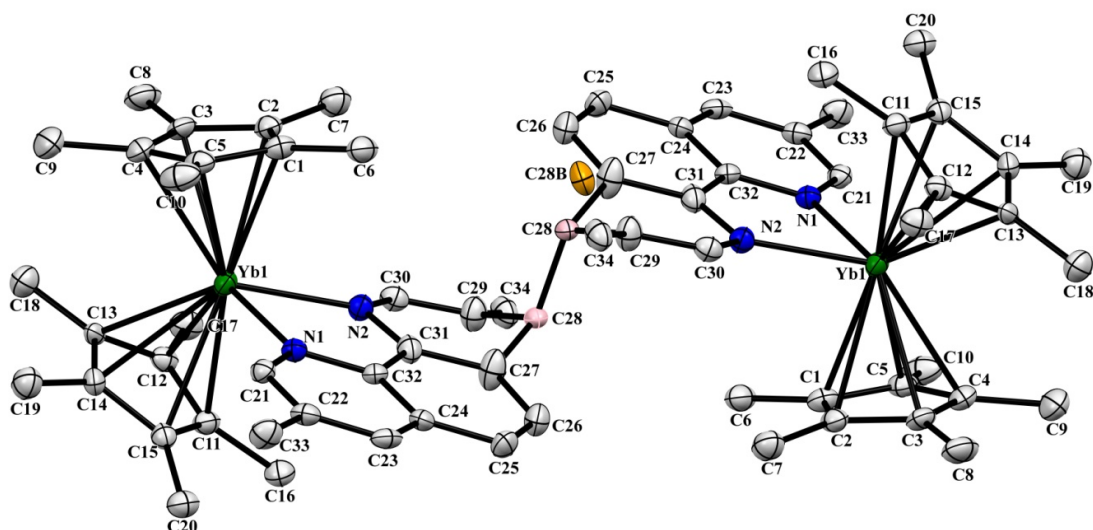


**Figure 9:** ORTEP for  $\text{Cp}^*_2\text{Yb}(3,8\text{-Me}_2\text{phen})$  (**3**). The carbon atom C28 (represented in pink) is refined in two positions C28 (2/3 of occupancy) and C(28B) is located in the plane of the phenanthroline closest to it. Details are in Supporting Information. Toluene molecules have been omitted for clarity.

These results provide a simple explanation for the questions raised by the solid state magnetic moments and EPR spectra of the neutral adducts. In **1-dimer** and **3-6**, the substituted phen radical anions are coupled forming a diamagnetic, dianionic ligand, which



bridges two cationic  $[\text{Cp}^*_2\text{Yb}]$  fragments. Accordingly, all of these compounds are EPR active, and their magnetic moments and XANES spectra are consistent with the presence of Yb(III). Only two compounds, **1-monomer** and **7**, actually contain radical anionic ligands, which can be seen in the increase in the magnetic moment of **1-monomer** relative to **1-dimer** and in the EPR inactivity of **7**.

Bond distances and angles in the phenanthroline adducts of ytterbocenes are shown in Table 4. The Yb-C( $\text{Cp}^*$ ) distances in the neutral and cationic adducts of  $\text{Cp}^*_2\text{Yb}$  are identical, given the large range in the individual values. The Yb-C( $\text{Cp}^*$ ) distances are approximately 0.1 Å shorter than in  $\text{Cp}^*_2\text{Yb}(\text{py})_2$ <sup>32</sup> and  $[1,3-(\text{Me}_3\text{Si})_2\text{C}_5\text{H}_3]\text{Yb}(\text{phen})$ <sup>14</sup> consistent with the higher oxidation number of ytterbium in the phenanthroline adducts of  $\text{Cp}^*_2\text{Yb}$ . It is particularly noteworthy that the Yb-C( $\text{Cp}^*$ ) distances are identical in the monomeric and dimeric forms of  $\text{Cp}^*_2\text{Yb}(\text{phen})$ .

The Yb-N distances, however, show significant differences in the neutral adducts depending upon whether they are monomers or dimers. In monomeric  $\text{Cp}^*_2\text{Yb}(\text{phen})$ , the average Yb-N distance is  $2.311 \pm 0.002$  Å, identical to that in  $\text{Cp}^*_2\text{Yb}(5,6\text{-Me}_2\text{phen})$  of  $2.318 \pm 0.007$  Å. In the dimeric forms of  $\text{Cp}^*_2\text{Yb}(\text{phen})$  and  $\text{Cp}^*_2\text{Yb}(3,8\text{-Me}_2\text{phen})$ , the average Yb-N distances of  $2.322 \pm 0.018$  Å and  $2.324 \pm 0.016$  Å are the same as those found in the monomers but the individual distances differ by 0.08 to 0.06 Å, respectively. Thus, the Yb-N(1) distances of  $2.358(5)$  Å and  $2.366(4)$  Å in **1-dimer** and **3**, respectively, are similar to those found in  $[\text{Cp}^*_2\text{Yb}(\text{phen})]\text{I}$  of  $2.339(8)$  Å and  $2.382(8)$  Å,<sup>14</sup> but the Yb-N(2) distances of  $2.285(4)$  Å and  $2.301(5)$  Å, respectively, are shorter and indicative of an amide-nitrogen to Yb(III) bond. This conjecture, *viz.*, that longer Yb-N bond lengths in the dimers are due to a Yb(III)-N (dative) and the shorter distances are due to a Yb(III)-N (anionic) bond is supported by comparison between the C-N and C-C bond distances in the individual pyridyl rings in **1-dimer** and **3** shown in Table 7 (see below). The trends in these bond lengths in the

phenanthroline rings in both dimers are consistent with the formulation of the N(1) pyridine ring as a neutral pyridine and the N(2) ring as 4-hydropyridyl, in which N(2) carries a negative charge. These bond lengths are in sharp contrast to those observed in the monomeric adducts,  $\text{Cp}^*_2\text{Yb}(\text{phen})$  and  $\text{Cp}^*_2\text{Yb}(5,6\text{-Me}_2\text{phen})$ , as shown in Table 8 (see below). In these two adducts, the small differences between C-N and C-C distances in the pyridine rings containing N(1) and N(2) are consistent with their formulation as delocalized radical anions.

**Table 4.** Bond lengths (Å) and Angles (deg) for the phenanthroline adducts of the Ytterbocenes.

Compound	Yb-C( $\text{Cp}^*$ ) <sup>(a)</sup> ave, Å	Yb-C <sub>t</sub> ave, Å	Yb-N ave, Å	Refs
$\text{Cp}^*_2\text{Yb}(\text{phen})$ , crystallized, (dimer)	$2.617 \pm 0.016$	2.33	2.285(4) 2.358(5)	This work
$\text{Cp}^*_2\text{Yb}(\text{phen})$ , sublimed, (monomer)	$2.610 \pm 0.008$	2.33	$2.311 \pm 0.002$	This work
$\text{Cp}^*_2\text{Yb}(3,8\text{-Me}_2\text{phen})$ , crystallized (dimer)	$2.63 \pm 0.02$	2.33	2.301(5) 2.366(4)	This work
$\text{Cp}^*_2\text{Yb}(5,6\text{-Me}_2\text{phen})$ , crystallized (monomer)	$2.62 \pm 0.02$		$2.330 \pm 0.005$	This work
Molecule 1	$2.63 \pm 0.01$	2.33	$2.322 \pm 0.005$	
Molecule 2	$2.63 \pm 0.01$	2.33	$2.313 \pm 0.005$	
Molecule 3	ave 2.63	2.33	ave 2.322	
$\text{Cp}^*_2\text{Yb}(5,6\text{-Me}_2\text{phen})$ , sublimed (monomer)	$2.620 \pm 0.005$	2.33	$2.310 \pm 0.009$	This work
$[\text{Cp}^*_2\text{Yb}(\text{phen})]\text{I}$	$2.61 \pm 0.01$	2.31	$2.360 \pm 0.011$	ref <sup>14</sup>
$[1,3\text{-(Me}_3\text{Si)}_2\text{C}_5\text{H}_3]\text{Yb}(\text{phen})$	$2.72 \pm 0.02$	2.43	$2.501 \pm 0.007$	ref <sup>14</sup>
$\text{Cp}^*_2\text{Yb}(\text{py})_2$	$2.74 \pm 0.04$		$2.565 \pm 0.005$	ref <sup>32</sup>

(a) the  $\pm$  values are average deviation from the mean values.

In the  $\text{Cp}^*_2\text{Yb}(\text{x},\text{x}'\text{-bipy})$  adducts, the changes in the C(2)-C(2') provide qualitative insights into the ground state electronic structure of these adducts.<sup>4,5</sup> In these charge-transfer complexes, the SOMO of the bipyridine radical-anion has  $b_1$  symmetry (in  $\text{C}_{2v}$  symmetry) and the C(2)-C(2') distance, represented by A in Scheme 1, shortens relative to the equivalent distance in the free bipyridine ligand, since these C- $p\pi$ -orbitals are a bonding combination. A related analysis of the C-N and C-C distances in the phenanthroline adducts is not as

straightforward since (i) the distance represented by A is part of a rigid-ring system and (ii) the LUMO and LUMO+1 orbitals of  $b_1$  and  $a_2$  symmetry (in  $C_{2v}$  symmetry), respectively, are close in energy, Figure 10, and population of these bonding and antibonding orbitals results in a complex pattern of bond length alterations since these  $p\pi$ -orbitals have different nodal properties and coefficients. However, a systematic examination of all the anticipated changes when either  $b_1$  or  $a_2$ -symmetry orbitals are singly occupied generates an informative pattern. The four pair of distances labeled as C and O; E and M; D and K; G and N in Scheme 1 change in identical ways when either  $b_1$  or  $a_2$  is singly occupied. In contrast the distances labeled A; I; F and L; B and P; H and J change in opposite directions as shown in Tables 5 and 6.

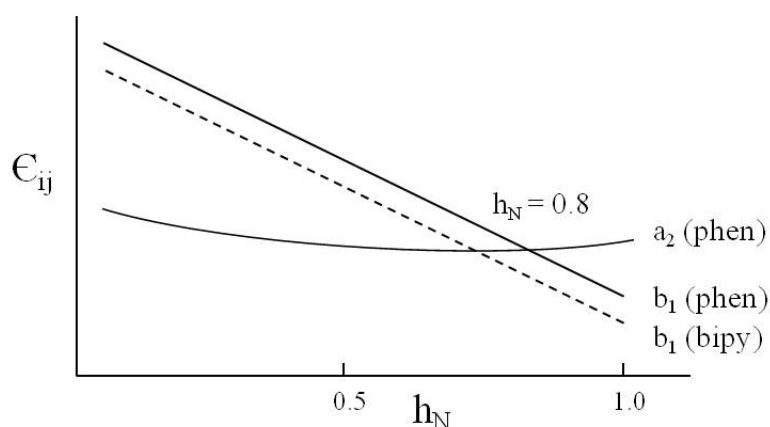


**Figure 10.** Relative energy diagram of the  $b_1$  and  $a_2$  symmetry orbitals in bipy radical anion and phen radical anion as a function of the Coulomb integral on N,  $h_N$ .<sup>41</sup>

**Scheme 1.**  $b_1$  and  $a_2$  representations and bond labeling.

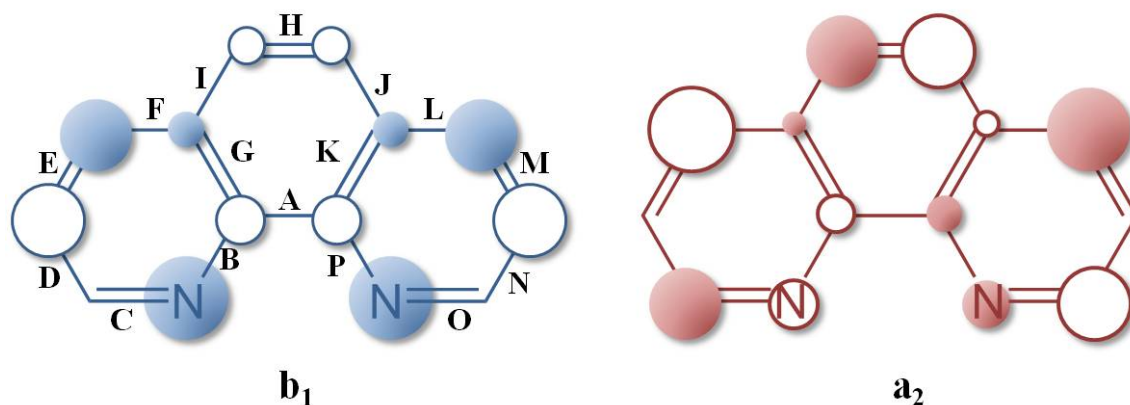


**Table 5.** Anticipated bond lengths changes in LUMO and LUMO+1 of phenanthroline radical anion.

Bond	Orbital <sup>(a)</sup>	
	LUMO, $b_1$	LUMO+1, $a_2$
A	-	+
I	-	+
F,L	-	+
B,P	+	-
H,J	+	-

(a) + means the distance increase, - means the distance decreases, when these orbitals are occupied.

**Table 6.** Bond lengths (Å) changes in **1-monomer** and **7**.

Bond	$\Delta^{(a,b)}$	
	Cp* <sub>2</sub> Yb(phen) monomer	Cp* <sub>2</sub> Yb(5,6-Me <sub>2</sub> phen) Monomers <sup>(c)</sup>
A	-0.020	-0.036
I	+0.014	-0.010
F,L	+0.041	-0.011
B,P	+0.003	+0.014
H,J	-0.026	-0.015

(a)  $\Delta$  is the bond length distance in the adduct minus that in the free ligand in Å.

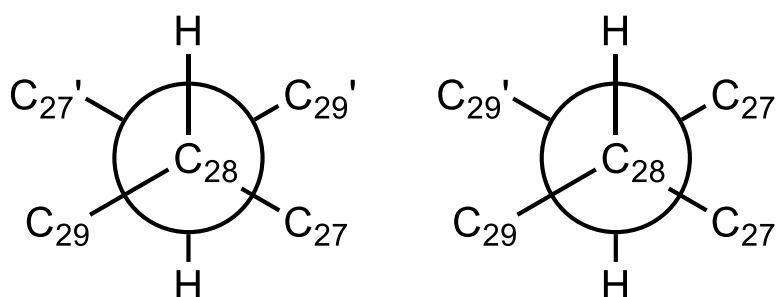
(b) Free phen, ref<sup>33</sup> and free 5,6-Me<sub>2</sub>phen, ref<sup>34</sup>

(c) The average change in the four individual molecules.

The pattern of bond length changes in monomeric  $\text{Cp}^*_2\text{Yb}(\text{phen})$  is inconsistent with population of either  $b_1$  or  $a_2$ -orbitals but consistent with population of both orbitals. The pattern of bond length alteration in  $\text{Cp}^*_2\text{Yb}(5,6\text{-Me}_2\text{phen})$  is somewhat different from that found in  $\text{Cp}^*_2\text{Yb}(\text{phen})$ , which implies that the  $b_1/a_2$  ratio is higher in the former adduct and that methyl groups in the 5,6-positions stabilize the  $b_1$  orbital. These inferences are consistent with the calculational results described below.

The geometry of the phenanthroline ligands in the two dimers,  $\text{Cp}^*_2\text{Yb}(\text{phen})$ , **1**, and  $\text{Cp}^*_2\text{Yb}(3,8\text{-Me}_2\text{phen})$ , **3**, is similar but the crystallographic details are different (Figure 8 and 9). In **1**, the C(28)-C(28') atoms have well-behaved thermal parameters, see Supporting Information, and these two carbon atoms are refined anisotropically although the hydrogen atoms attached to them are not included in the refinement. The geometry of the N(1)-ring in the  $\text{Cp}^*_2\text{Yb}(\text{phen})$  is planar while that of the N(2)-ring is non-planar. In the N(2)-ring, the dihedral angle formed by intersection of the two planes defined N(2)C(30)C(29)C(27)C(31) and C(27)C(28)C(29) is  $25^\circ$ , in accord with C(28) being a  $\text{sp}^3$ -carbon atom. The C(28)-C(27,29) distances in Table 7 are in the range given for  $\text{Csp}^3\text{-Csp}^3$  bond lengths of  $1.507 \text{ \AA}$  ( $\sigma = 0.015 \text{ \AA}$ ).<sup>35</sup> The C – N distances, Table 7, are also in the range of  $\text{Csp}^3\text{-N}$  distances of  $1.358 \text{ \AA}$  ( $\sigma = 0.015 \text{ \AA}$ ).<sup>35</sup> These distances and angles in the N(2)-ring indicate that the pyridyl ring is represented by a quinoid distortion and the nitrogen atom carries a negative charge.

**Scheme 2.**



The orientation of the two phenanthrolyl rings in the crystal structure is shown by the Newman projection down the C(28)C(28') bond, Scheme 2, left-hand drawing. The molecule

has  $C_i$  symmetry and the inversion center is the mid-point of C(28)C(28'). The Newman projection of another rotomer of  $C_2$  symmetry is shown in the right-hand drawing.

**Table 7.** C-N and C-C bond distances in **1-dimer** and **3**

Cp* <sub>2</sub> Yb(phen), <sup>c</sup> <b>1-dimer</b>				
Ring 1 <sup>a</sup>		Ring 2 <sup>b</sup>		$\Delta^e$
Bond <sup>c</sup>	Distance, Å	Bond	Distance, Å	
N(1)C(21)	1.331(7)	N(2)C(30)	1.380(7)	-0.049
N(1)C(32)	1.396(6)	N(2)C(31)	1.374(7)	+0.022
C(21)C(22)	1.393(8)	C(30)C(29)	1.336(8)	+0.067
C(22)C(23)	1.375(9)	C(29)C(28)	1.504(8)	-0.129
C(23)C(24)	1.417(9)	C(28)C(27)	1.500(8)	-0.083
C(24)C(32)	1.387(7)	C(27)C(31)	1.413(7)	-0.024

Cp* <sub>2</sub> Yb(3,8-Me <sub>2</sub> phen), <sup>c</sup> <b>3</b>				
Ring 1 <sup>a</sup>		Ring 2 <sup>b</sup>		$\Delta^e$
Bond <sup>c</sup>	Distance, Å	Bond	Distance, Å	
N(1)C(21)	1.339(6)	N(2)C(30)	1.381(6)	-0.042
N(1)C(32)	1.384(6)	N(2)C(31)	1.374(6)	+0.010
C(21)C(22)	1.399(7)	C(30)C(29)	1.352(7)	+0.047
C(22)C(23)	1.388(7)	C(29)C(28)	1.529(9)	-0.141
C(23)C(24)	1.394(7)	C(28)C(27)	1.547(9)	-0.153
C(24)C(32)	1.419(7)	C(27)C(31)	1.403(7)	+0.016

**Table 8.** C-N and C-C bond distances in **1-monomer** and **7**.

Cp* <sub>2</sub> Yb(phen), <sup>d</sup> <b>1-monomer</b>				
Ring 1 <sup>a</sup>		Ring 2 <sup>b</sup>		$\Delta^e$
Bond	Distance, Å	Bond	Distance, Å	
N(1)C(21)	1.383(6)	N(2)C(30)	1.381(7)	+0.002
N(1)C(32)	1.367(5)	N(2)C(31)	1.365(6)	+0.002
C(21)C(22)	1.371(9)	C(30)C(29)	1.382(8)	-0.011
C(22)C(23)	1.388(9)	C(29)C(28)	1.392(9)	-0.004
C(23)C(24)	1.459(8)	C(28)C(27)	1.445(8)	+0.013
C(24)C(32)	1.414(7)	C(27)C(31)	1.426(6)	-0.012

Cp* <sub>2</sub> Yb(5,6-Me <sub>2</sub> phen), <sup>d</sup> <b>7-monomers</b> (average)				
Ring 1 <sup>a</sup>		Ring 2 <sup>b</sup>		$\Delta^e$
Bond <sup>c</sup>	Distance, Å	Bond	Distance, Å	
N(1)C(21)	1.350(11)	N(2)C(30)	1.352(7)	-0.002
N(1)C(32)	1.377(7)	N(2)C(31)	1.371(15)	+0.006
C(21)C(22)	1.369(12)	C(30)C(29)	1.370(8)	-0.001
C(22)C(23)	1.388(16)	C(29)C(28)	1.380(7)	+0.008
C(23)C(24)	1.40(3)	C(28)C(27)	1.40(2)	0.0
C(24)C(32)	1.423(8)	C(27)C(31)	1.428(10)	-0.005

a) Ring 1 are the atoms in the ring defined by N(1).

b) Ring 2 are the atoms in the ring defined by N(2).

c) See Figure 8 and 9 for the atom numbering scheme.

d) See Figure 5 and 7 for the atom numbering scheme.

e) The differences in Å between the distances in ring 1 and ring 2.

The description of the geometry around C(28) in the  $\text{Cp}^*_2\text{Yb}(3,8\text{-Me}_2\text{phen})$ , **3** is less straightforward since two positions for the C(28) atom are occupied (C(28) and C(28B)). While solving the structure, a singularity appeared at atom C28. The problem is addressed in two ways: (i) the C28 atom is forced to remain in the mean plane of ring 2 and (ii) a positional disorder model in which C28 and C28B are assigned an occupancy ratio of 0.67:0.33, respectively. Solution (i) led to an elongated thermal ellipsoid perpendicular to the mean plane of ring 2, Figure S22 representing this tentative solution is shown in the Supporting Information. In this representation the C(28)C(28') distance is 3.00 Å. Solution (ii) led to well-behaved thermal ellipsoids for C(28) and C(28B) but their position differs; C(28) is comparable to that of the C(28) atom in **1-dimer** with elongated C(28)-C(29,27) distances (see Table 7) of 1.529(9) Å and 1.547(9) Å, respectively, and a C(28)-C(28') distance of 1.592(16) Å. This is compatible with the presence of a  $\sigma$ -dimer, that is the bond between C(28)C(28') is classified as a  $\sigma$ -bond between two  $\text{sp}^3$  carbons. On the other hand, C(28B) is found close to the mean plane of ring 2 with C(28B)C(29,27) distances of 1.478(18) Å and 1.417(19) Å and a C(28B)C(28B') distance of 3.39 Å (calculated), compatible with its classification as a  $\pi$ -dimer, that is, a bond formed by interaction between the  $p_z$ -orbitals on the  $\text{sp}^2$  hybridized carbon atoms. The disorder in  $\text{Cp}^*_2\text{Yb}(3,8\text{-Me}_2\text{phen})$ , **3**, may be viewed as the average between these two forms ( $\sigma$ -dimer and  $\pi$ -dimer) in which the energy difference between them is small.

### Vis-NIR Spectra.

The Vis-NIR spectra in the 400-950 nm range in toluene solution at 20 °C for the crystallized adducts of 4-Mephen (**5**) and 5-Mephen (**6**) are similar to the spectrum of  $\text{Cp}^*_2\text{Yb}(\text{phen})$  (**1**) reported in an earlier paper.<sup>14</sup> The spectra are available in SI. Morris and co-workers have given a detailed analysis of the solution spectra from 400 nm to 2500 nm of  $[\text{Cp}^*_2\text{Yb}(\text{phen})]^{0,+6}$ . The key point that emerges from these spectroscopic studies is that the



spectra of the neutral adducts contain features associated with the phenanthroline radical anion, an absorption around 500 nm, along with f-f transitions at longer wavelengths.

### **<sup>1</sup>H NMR Spectra.**

The chemical shifts in C<sub>6</sub>D<sub>6</sub> or C<sub>7</sub>D<sub>8</sub> at 300 K for the neutral adducts are given and assigned in Table 9. The Cp\*<sub>2</sub>Yb(phen), Cp\*<sub>2</sub>Yb(3,8-Me<sub>2</sub>phen) and Cp\*<sub>2</sub>Yb(5,6-Me<sub>2</sub>phen) adducts have four resonances due to the phenanthroline ligands in the general region of  $\delta H \sim 100$ ,  $\sim 50$ ,  $\sim 15$  and  $\sim 0$  ppm, in addition to the Cp\* resonance at  $\delta H \sim 4$  ppm. The resonances that can be assigned with certainty are those at  $\delta H \sim 15$  ppm since these are replaced by a resonance due to the Me-groups at  $\delta H \sim -10$  ppm in **3**, and therefore the  $\delta H \sim 15$  ppm resonance is due to  $\delta_{3,8}$ . The resonances at  $\delta H \sim 0.5$  ppm are replaced by a resonance due to the Me-groups at  $\delta H \sim 0.03$  ppm in **7**, and therefore the  $\delta H \sim 0.5$  ppm is due to  $\delta_{5,6}$ . The most deshielded resonances are assigned to  $\delta_{2,9}$  since these are closest to the paramagnetic center, and the remaining resonances at  $\delta H \sim 50$  ppm are due to  $\delta_{4,7}$ . The appearance of four phen resonances shows that the adducts have C<sub>2v</sub> symmetry in solution at 300 K. The chemical shifts of Cp\*<sub>2</sub>Yb(3,8-Me<sub>2</sub>phen) depend upon the solvent; in THF the most downfield resonance in C<sub>7</sub>D<sub>8</sub> moves upfield by about 20 ppm while the other resonances shift by a lesser amount (see Experimental Section). The eight resonances in the 5-Mephen adduct are consistent with a single isomer of C<sub>s</sub> symmetry at 300 K but those in the 4-Mephen adduct are not observed at 300 K, while only some of the resonances for the 3-Mephen adduct are observed. The low solubility of the neutral adducts precludes a more detailed study with exception of the 3,8-Me<sub>2</sub>phen and 5,6-Me<sub>2</sub>phen adducts that are somewhat more soluble in THF and toluene.

**Table 9.**  $^1\text{H}$  NMR chemical shift in  $\text{C}_6\text{D}_6$  or  $\text{C}_7\text{D}_8$  at 300 K for neutral adducts **1**, **3-7**.

Compound	2,9	4,7	3,8	5,6	Cp*
$\text{Cp}^*_2\text{Yb}(\text{phen})$ ( <b>1</b> )	139.94	47.87	14.02	0.47	4.14
$\text{Cp}^*_2\text{Yb}(3,8\text{-Me}_2\text{phen})$ ( <b>3</b> )	95.54	51.07	-10.03 (Me)	3.83	3.36
$\text{Cp}^*_2\text{Yb}(3\text{-Mephen})$ ( <b>4</b> )	121.47	59.15	18.69	-	3.79
	118.38	57.17	-9.51 (Me)	-	
$\text{Cp}^*_2\text{Yb}(4\text{-Mephen})$ ( <b>5</b> )	-	-	-	-	4.03
$\text{Cp}^*_2\text{Yb}(5\text{-Mephen})$ ( <b>6</b> )	138.72	47.92	14.18	0.06	4.09
	138.59	39.33	11.40	-0.58 (Me)	
$\text{Cp}^*_2\text{Yb}(5,6\text{-Me}_2\text{phen})$ ( <b>7</b> )	137.44	44.10	14.66	0.03 (Me)	3.95

**Variable temperature  $^1\text{H}$  NMR of  $\text{Cp}^*_2\text{Yb}(3,8\text{-Me}_2\text{phen})$  (**3**).**

Dissolution of the crystals of the complex **3** in toluene and THF is kinetically slow, in agreement with strong packing forces in the solid state, but gently warming ( $60^\circ\text{C}$ ) the solution over a period of one or two days gives saturated solutions that allow  $^1\text{H}$  NMR spectroscopic measurements at variable temperatures. At room temperature, both toluene- $\text{d}_8$  and THF- $\text{d}_8$  solution of **3** are deep red and show one major set of 5 resonances in a 2:2:2:30:6 ratio. This is in agreement with the presence of monomeric  $\text{Cp}^*_2\text{Yb}(3,8\text{-Me}_2\text{phen})$  with  $\text{C}_{2v}$  symmetry in which the phenanthroline ligand is symmetrically disposed relative to the  $\text{Cp}^*_2\text{Yb}$  fragment and these resonances are designated by the letter S for “symmetric”. Small resonances are also present, contributing less than 5% of the peak intensity. When the toluene- $\text{d}_8$  and THF- $\text{d}_8$  solution are cooled, these low-intensity resonances grow at the expense of the resonances assigned to the monomeric  $\text{Cp}^*_2\text{Yb}(3,8\text{-Me}_2\text{phen})$  complex (S). The solutions change color from deep red at room temperature to purple at 250 K and blue at 200 K. The  $^1\text{H}$  NMR spectra at low temperature in both solvents show three different sets of resonances; one set of 5 resonances attributed to the S isomer, the monomeric form of **3**, and in two other sets of resonances, labeled  $\text{A}_1$  and  $\text{A}_2$  (A for asymmetric), in which the methyl resonances are not equivalent, in agreement with the formation of a dimer, Figure 9 and

Scheme 2. Ten resonances are expected for each isomer in a ratio 2:2:2:2:2:2:6:6:30, although some resonances were not located in a -100 to 100 ppm window. The ratio of the two asymmetric isomers A<sub>1</sub> and A<sub>2</sub> is approximately 60:40 in toluene and 55:45 in THF and the ratio is only slightly dependent on temperature, given the errors of the integration.

Two pairs of A resonances are attributed to the methyl groups based on the integration ratio and are highlighted by the red dots in Figure 11. These resonances are integrated and related to the S-methyl resonance that is highlighted by a blue dot in Figure 11. The relative change in population of these methyl group resonances is used to obtain the van't Hoff plot in Figure 12; the details are provided in the Experimental Section. The thermodynamic parameters for the equilibrium shown in Eq. 2, where M is the symmetric (S), monomer and D the asymmetric (A<sub>1</sub> + A<sub>2</sub>), dimer, set of resonances, are determined from this plot.



The resulting  $\Delta H$  values are -5.8 kcal/mol and -8.1 kcal/mol in THF and toluene, respectively, and the  $\Delta S$  values are -26 kcal/mol/K and -31 kcal/mol/K in THF and toluene, respectively. At 298 K, the value of the dimerization constant ( $K_1$ ) is  $0.05 \pm 0.005 \text{ M}^{-1}$  in THF and  $0.48 \pm 0.01 \text{ M}^{-1}$  in toluene. A similar pattern of  $\Delta H$  and  $\Delta S$  values are reported by Kochi and co-workers for the  $\pi$ -radical tricyclic phenalenyl.<sup>36</sup> When a large excess of dihydroanthracene is added to a C<sub>7</sub>D<sub>8</sub> solution of Cp\*<sub>2</sub>Yb(phen) and heated to 60 °C for a period of two days, no anthracene is formed, implying that the phenanthrolyl radical does not behave as a free radical.

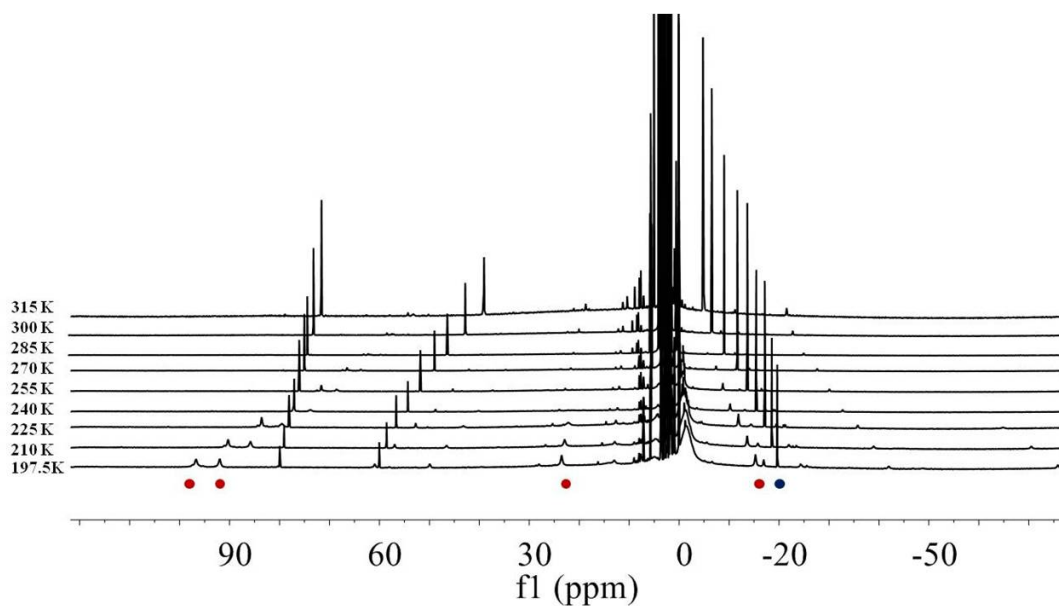


**Figure 11.** Stacked plot of  $^1\text{H}$  NMR spectra in function of the temperature in THF. Red dots are the resonances used for integration of the asymmetric species and the blue dot for the symmetrical species.

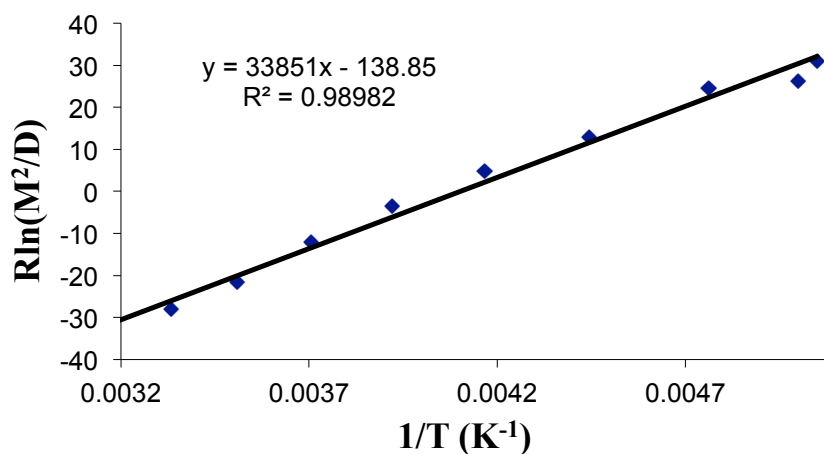


**Figure 12.** van't Hoff plot of the equilibrium reaction  $2\text{M} = \text{D}$  in toluene (M is **3** as a monomer, D corresponds to the the two dimeric isomers). The plot of  $R\ln(K)$  ( $K_1 = \text{D}/\text{M}^2$ ) vs.  $1/T$  yields  $\Delta H^0 = -8.1(2)$  kcal/mol,  $\Delta S^0 = -31(1)$  cal/mol/K and  $K_1$  ( $25^\circ\text{C}$ ) =  $0.48 \text{ M}^{-1}$ .

## Calculations.

The CASSCF methodology used in previous papers for the bipyridine adducts of  $\text{Cp}^*_2\text{Yb}$  is extended to the monomeric phenanthroline adducts,  $\text{Cp}^*_2\text{Yb}(\text{phen})$  (**1**),  $\text{Cp}^*_2\text{Yb}(3,8\text{-Me}_2\text{phen})$  (**3**) and  $\text{Cp}^*_2\text{Yb}(5,6\text{-Me}_2\text{phen})$  (**7**). The calculated ground state of  $\text{Cp}^*_2\text{Yb}(\text{phen})$  is comprised of two nearly degenerate triplet states,  $T_1$  and  $T_2$ , which are 2.12 eV lower in energy than an open-shell singlet state. The state configuration for the f-orbitals are therefore pure (100 %)  $f^{13}$  and the  $T_1$  and  $T_2$  configuration for the  $\pi^*$ -orbitals are  $0.72 \pi^*_1 + 0.28 \pi^*_2$  and  $0.28 \pi^*_1 + 0.72 \pi^*_2$ , respectively. The calculated charge-transfer ground state is in accord with the observation of two LMCT bands near  $500 \text{ cm}^{-1}$  in the Vis-NIR spectrum in toluene solution.<sup>6</sup> The calculated ground states for the 3,8- $\text{Me}_2\text{phen}$  and 5,6- $\text{Me}_2\text{phen}$  adducts are similar to each other but somewhat different than that of the unsubstituted phenanthroline adduct. Thus, the calculated ground states are spin triplets (pure  $f^{13}$ ) but the open-shell singlet states are only 0.08 eV and 0.09 eV higher in energy, respectively. The excited-state open-shell singlets are multiconfigurational in which the dominant configuration is  $f^{13}$ ; in 3,8- $\text{Me}_2\text{phen}$ , the  $f^{13}:f^{14}$  contributions are 0.75:0.25 and the  $\pi^*_1$  is the only configuration that contributes. In the 5,6- $\text{Me}_2\text{phen}$  adduct, the  $f^{13}:f^{14}$  contributions in the excited open-shell singlet state are 0.85:0.15 and the  $\pi^*_1$  and  $\pi^*_2$  contributions are 0.95 and 0.05, respectively. The calculated spin triplet ground states in these three phenanthroline adducts are in dramatic contrast with the open-shell singlet ground states obtained in all the bipyridine adducts of  $\text{Cp}^*_2\text{Yb}$ . The calculated singlet-triplet separation is 0.28 eV in  $\text{Cp}^*_2\text{Yb}(\text{bipy})$ , singlet lowest and 2.12 eV in  $\text{Cp}^*_2\text{Yb}(\text{phen})$  with the triplet lowest. Thus the triplet energies and therefore the ground state electronic structure change by 2.4 eV, about  $60 \text{ kcal.mol}^{-1}$ , just by changing the ligands.

The dimerization reaction is studied by DFT calculations. The  $\text{Cp}^*$  rings are replaced by Cp in these calculations since the full system for the dimer is prohibitively large. A

transition state is calculated to be 15.4 kcal.mol<sup>-1</sup> (in Gibbs energy) above the monomers and the dimerization reaction is exoergic by 3.1 kcal.mol<sup>-1</sup> (Figure 13), consistent with the experiential observation that Cp\*<sub>2</sub>Yb(phen) is a dimer. The calculated distance of the C-C bond formed in 4,4'-positions (1.596 Å) is in resonable agreement with the elongated C-C bond found in the solid state structure (1.619 Å). The transition state; Figure S26, involves two molecules of Cp<sub>2</sub>Yb(phen) with similar bond distances as calculated for the dimer, but with a C-C bond distance of 1.800 Å.

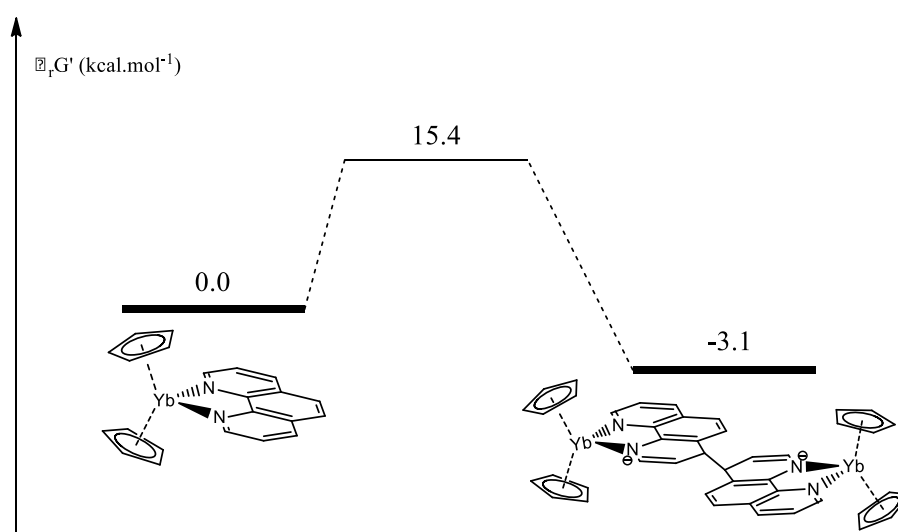


**Figure 13.** Reaction coordinate diagram for dimerization of Cp<sub>2</sub>Yb(phen).

## Discussion.

Although the molecular geometry of monomeric Cp\*<sub>2</sub>Yb(phen) is similar to that found in the wide range of bipyridine adducts, their electronic structures are different.<sup>4,5,14</sup> The ground state electronic structure of the bipyridine adducts are open-shell singlets that are multiconfigurational in which the ground state wave function,  $\Psi$ , is  $C_1|f^{13}, \text{bipy}^-> + C_2|f^{14}, \text{bipy}>$ , where  $C_1$  and  $C_2$  are coefficients of the two configurations. For Cp\*<sub>2</sub>Yb(bipy),  $C_1^2 = 0.83$ .<sup>4</sup> This results in the ytterbium atom being intermediate valent, that is, it is neither Yb(III),  $f^{13}$ , nor Yb(II),  $f^{14}$  but in between these extreme values in which the  $f^{13}$  configuration is dominant. The open-shell singlet ground state (or states) determines the magnetic properties

of these adducts, and in the case of the 4,5-diazafluorene adduct, is postulated to be the origin of the chemical reactivity.<sup>37</sup>

In contrast, the monomeric phenanthroline adducts  $\text{Cp}^*_2\text{Yb}(\text{phen})$  and  $\text{Cp}^*_2\text{Yb}(5,6\text{-Me}_2\text{phen})$  have open-shell triplet ground states, and the valence of ytterbium is fully trivalent. The CASSCF computational studies indicate that two open-shell triplets are nearly degenerate and are some 2 eV lower in energy than the open-shell singlet state, consistent with the magnetic studies and the L-III edge XANES. A model that accounts for the different electronic ground states in the bipy and phen adducts is outlined next; the model is offered as a qualitative guide for what is known and as a guide for future experimental studies.

Whether a monomeric ytterbocene diimine complex has a triplet or singlet ground state is largely governed by kinetic exchange, that is, by mixing of excited state configurations into the ground state.<sup>38,39</sup> The interaction between the half-occupied ligand orbital and a half-occupied 4f-orbital stabilizes the singlet state while interactions between the half-occupied ligand orbital and the empty metal based orbitals on the  $\text{Cp}^*_2\text{Yb}$  fragment, especially the 5d-orbitals, stabilize the triplet state. To a first approximation, the strength of the interactions between the half-occupied ligand orbital and the metal orbitals are proportional to the square of the overlap and inversely proportional to the difference in energy between the ligand and metal orbitals. Since the overlap between the ligand orbitals and the Yb 5d orbitals is anticipated to be significantly larger than the overlap with the Yb 4f orbitals, whether the ground state is a singlet or triplet depends in large part on the energies of the ligand orbitals.<sup>40</sup> If the half-occupied ligand orbital is close in energy to the 4f-orbitals and has the proper symmetry to overlap with the lone half-filled Yb 4f-orbital, the singlet state is likely to be lowest in energy. However, if the half-occupied ligand orbital is not close in energy to the 4f orbitals or does not have the proper symmetry to overlap with the half-occupied Yb 4f orbital, the interaction between the half-occupied ligand orbital and the Yb 5d orbitals will be

stronger, and the triplet state will be stabilized. If the ligand has empty orbitals close in energy to the half-occupied orbital, the ground state could be either a singlet or triplet depending on whether the interaction between the ligand orbitals and the singly occupied 4f-orbital is greater or weaker than the interactions with the empty 5d orbitals.

In  $\text{Cp}^*_2\text{Yb}(\text{bipy})$ , the open-shell singlet is calculated to be 0.28 eV below the triplet and the experimental value of the singlet-triplet energy difference is about 0.1 eV by comparing to the Hubbard model.<sup>11</sup> When an f-electron is transferred to the LUMO, only one of the four possible  $\pi^*$ -orbitals, the  $b_1$ -orbital, is of sufficiently low energy to be populated and the unpaired spin density is distributed among the  $p\pi$ -orbitals on the C and N atoms of the bipyridine ligand. In this case, the half-occupied ligand orbital and the half-occupied Yb 4f orbital are close in energy and have the same symmetry,  $b_1$ , so the kinetic exchange configuration interaction stabilizes the open-shell singlet. This model fits all of the experimental and computational studies associated with the bipy adducts.<sup>4,5</sup>

In contrast, the LUMO and LUMO+1 of phenanthroline are close in energy (Figure 10, Chart 1) so that when electron transfer occurs, the electron occupies either the  $\pi^*_1$  and/or  $\pi^*_2$  orbitals, which have  $b_1$  and  $a_2$  symmetry, respectively (in  $C_{2v}$  symmetry). The ordering of these orbitals can be inverted by methyl group substituents in the solvent separated radical-anions as shown by EPR studies. Thus  $\text{phen}^-$ ,<sup>41</sup>  $2,9\text{-Me}_2\text{phen}^-$ ,<sup>42</sup>  $4,7\text{-Me}_2\text{phen}^-$ <sup>41</sup> and  $5,6\text{-Me}_2\text{phen}^-$ <sup>42</sup> have  $^2B_1$  ground states but  $3,4,7,8\text{-Me}_4\text{phen}^-$  has a  $^2A_2$  ground state.<sup>43</sup> As in  $\text{Cp}^*_2\text{Yb}(\text{bipy})$ , the  $b_1$  orbital will be stabilized by interaction with the half-filled Yb 4f-orbital, which stabilizes the singlet state. This assumes that the orbital from which the electron on the close-shell  $\text{Cp}^*_2\text{Yb}$  metallocene is removed does not undergo reorganization, that is, the hole remains in a  $b_1$  symmetry orbital. The  $a_2$  orbital will not be stabilized by Yb 4f-orbitals since the single half-occupied orbital has  $b_1$  symmetry. The ligand  $a_2$  orbital can be stabilized by interaction with the empty Yb 5d orbitals. If the  $a_2$  orbital is half-occupied, the triplet ground



state will be stabilized, which is the case for all of the monomeric ytterbocene phenanthroline complexes reported here.

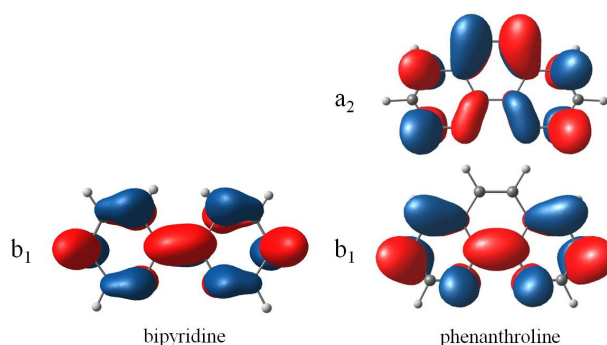


**Chart 1.**

The difference between the bipyridine and phenanthroline adducts can be illustrated using a MO diagram as illustrated in Figure 14. While the MO model does not capture the stabilization of the triplet or singlet state due to configuration interaction, the stable spin state is indicated by the relative spins of the electrons as indicated by the arrows in Figure 14. Figure 14 illustrates two extreme cases that are possible for two spins. This diagram may be extended to the specific examples of  $\text{Cp}^*_2\text{Yb}(\text{diimine})$  since the symmetry orbitals of bent sandwich metallocenes are well known.<sup>44,45</sup> The d-orbitals that are empty, once the diimine  $\sigma$ -bonds are created, are the non-bonding  $a_1(d_{x^2-y^2})$  metal-based orbital and the higher lying  $\text{Cp}^*\text{-Yb}$  antibonding  $d_{xy,yz}$  orbitals of  $b_1$  and  $a_2$  symmetry. The seven f-orbitals occupied by 13 electrons are considered to be non-bonding and much lower in energy than the d-parentage orbitals. In the bipy adducts, Figure 14, left-hand side, the hole in the f-orbitals has  $b_1$ -symmetry as does the electron in the ligand-based orbital. As these two electrons have the same symmetry, they can mix to give a singlet state, following the Pauli principle. This model accounts for the electronic ground states of  $\text{Cp}^*_2\text{Yb}(\text{bipy})$ .<sup>4,5</sup>

Extending this MO model to the phenanthroline adducts is complicated by the fact that either the  $b_1$  or  $a_2$  orbitals or both are populated depending upon their relative energies, Figure

10. Thus, three idealized cases may be considered, (i)  $b_1$  lies lower than  $a_2$ , (ii)  $a_2$  lies lower than  $b_1$ , and (iii)  $b_1$  and  $a_2$  are of similar energy. Case (i) results in an orbital pattern found in bipy, Figure 14, left-hand side. Case (ii) results in a similar orbital pattern, except that the  $b_1$  and  $a_2$  orbital are interchanged. Both of these cases can result in singlet ground states. Case (iii), Figure 14, right-hand side, is applicable to the phen adducts described above. Thus, an electron in the  $a_2$ -ligand-based orbital is stabilized by interaction with a  $d_{xy}$  orbital of  $a_2$  symmetry on the  $\text{Cp}^*_2\text{Yb}$  metallocene resulting in the  $a_2$ -MO below the  $b_1$ -MO, resulting in a spin-triplet ground state, since the hole in the f-manifold is in a  $b_1$  symmetry orbital. Case (iii) illustrate how methyl substituents change the relative energies of the  $b_1$  and  $a_2$ -orbitals generating a model for how the magnetic properties are controlled by the  $b_1$ - $a_2$  separation.

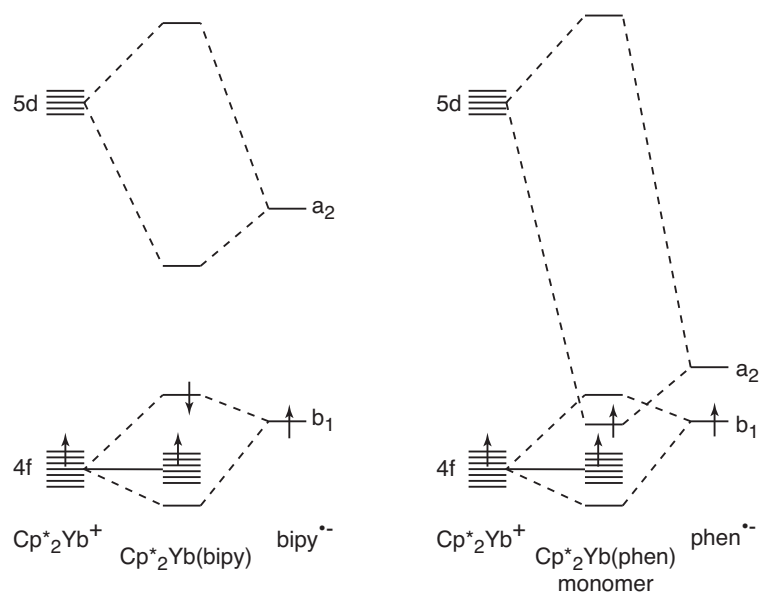


**Figure 14.** Qualitative MO diagram comparing bonding in  $\text{Cp}^*_2\text{Yb}(\text{bipy})$  and  $\text{Cp}^*_2\text{Yb}(\text{phen})$  monomer. Only the unpaired 4f electron is illustrated; the orbitals below those with arrows are filled. The direction of the arrows indicate the ground state:  $\text{Cp}^*_2\text{Yb}(\text{bipy})$  has a singlet ground state while  $\text{Cp}^*_2\text{Yb}(\text{phen})$  has a triplet ground state.

Inspection of the  $b_1$ -orbital in  $\text{phen}^{\bullet-}$  shows that the spin density is more likely to reside on N, C(2,9), C(3,8), and C(4,7) whereas in the  $a_2$ -orbital the spin density is likely to be found on C(2,9), C(4,7) and C(5,6), chart 1. Thus, the unpaired spin density on N is greater in

the  $b_1$ -orbital than in the  $a_2$ -orbital. Population of the  $a_2$ -orbital increases spin density on  $p\pi$ -orbitals of C(4,7), which is the site of C-C bond formation in the dimer. Thus, substituents on the phenanthroline ring in the ytterbocene adducts modulates the unpaired spin density of the  $p\pi$ -orbitals and the radical character at a given site and therefore the site at which chemical reactions occurs.

Dimerization of two  $\sigma$ -carbon radicals forming a  $\sigma$ -C<sub>2</sub> single bond involves two enthalpy changes with opposite signs. The exothermic term involves C-C bond formation, about 80-85 kcal.mol<sup>-1</sup>, and the endothermic term is due to loss of resonance stabilization in the  $\sigma$ -radical, estimated to be about 35 kcal.mol<sup>-1</sup> per radical.<sup>36</sup> The net enthalpy changes favor dimerization but loss of entropy results in  $\Delta G$  being close to zero.

## Conclusion.

The key conclusion in this article is that the electronic ground states for Cp\*<sub>2</sub>Yb(phen), the 3,8-, and the 5,6-dimethyl adducts are different from those of Cp\*<sub>2</sub>Yb(bipy) and its methyl and dimethyl-substituted adducts; the ground state of monomeric Cp\*<sub>2</sub>Yb(phen) and its adducts is a spin triplet and the valence of ytterbium is trivalent. In contrast, the ground state of Cp\*<sub>2</sub>Yb(bipy) is a multiconfigurational open-shell singlet and ytterbium is intermediate valent. The chemical manifestation of this difference is that the solid state structure of the sublimed phenanthroline adduct is a monomer but that of the crystallized adduct is a dimer in which the phenanthroline ligands are coupled by formation of a C-C bond between the carbons at the 4-position. The 3,8-Me<sub>2</sub>phenanthroline adduct is similar but in this case the monomer and dimer are in equilibrium in toluene-d<sub>8</sub> or in tetrahydrofuran-d<sub>8</sub> with values of  $\Delta H$  of -8.1 kcal/mol and -5.8 kcal/mol, respectively, and  $\Delta S$  values of -31 kcal/mol/K and -26 kcal/mol/K, respectively. The origin of the different physical and chemical properties is postulated to arise from the different symmetry orbitals available in the phen<sup>•-</sup> and bipy<sup>•-</sup>; the former has two accessible orbitals of  $b_1$  and  $a_2$  symmetry (in C<sub>2v</sub>) while the later has only one

of  $b_1$  symmetry. Even though the ground state electronic structure of  $\text{Cp}^*_2\text{Yb}(\text{bipy})$  and  $\text{Cp}^*_2\text{Yb}(\text{phen})$  are different, the solution (thf) electrochemistry study of these two adducts shows that both of the charge-transfer ground states are stabilized by the same amount, 0.79 V ( $18.4 \text{ kcal.mol}^{-1}$ ) relative to  $\text{Cp}^*_2\text{Yb}(\text{II})$  in thf.<sup>6</sup> This difference results in the same value of the comproportionation constant,  $K_c = 10^{-13.4}$  for each adduct, eq. 3.



At first glance, this thermodynamic statement is surprising, however, the major contribution to the bond enthalpy in both adducts is from interaction between the cationic and anionic fragments, and the change in electronic structure is a small contribution to  $\Delta G$ .

### Experimental.

**General considerations.** All reactions were performed using standard Schlenk-line techniques or in a drybox (MBraun). All glassware was dried at  $150^\circ\text{C}$  for at least 12 h prior to use. Toluene, pentane and diethyl ether were dried over sodium and distilled while  $\text{CH}_2\text{Cl}_2$  was purified by passage through a column of activated alumina. Toluene- $d_8$  was dried over sodium and  $\text{CH}_2\text{Cl}_2-d_2$  was dried over calcium hydride. All the solvents were degassed prior to use.  $^1\text{H}$  NMR spectra were recorded on Bruker AVB-400 MHz, DRX-500 MHz, AVB-600 MHz and Avance 300 MHz spectrometers.  $^1\text{H}$  chemical shifts are in  $\delta$  units relative to TMS, and coupling constants ( $J$ ) are given in Hz. Infrared spectra were recorded as Nujol mulls between KBr plates on a Thermo Scientific Nicolet IS10 spectrometer. Samples for UV-Vis-NIR spectroscopy were contained in a Schlenk-adapted quartz cuvette and obtained on a Varian Cary 50 scanning spectrometer. Melting points were determined in sealed capillaries prepared under nitrogen and are uncorrected. Elemental analyses were determined at the Microanalytical Laboratory of the College of Chemistry, University of California, Berkeley. X-ray structural determinations were performed at CHEXRAY, University of California, Berkeley. Magnetic susceptibility measurements were made for all samples at 1, 5 and 40 kOe

in a 7 T Quantum Design Magnetic Properties Measurement System that utilizes a superconducting quantum interference device (SQUID). Sample containment and other experimental details have been described previously.<sup>46</sup> It is important to note that the susceptibility values obtained when the samples were contained in Kef-F containers and quartz tube are identical within experimental errors.<sup>14</sup> Diamagnetic corrections were made using Pascal's constants. The samples were prepared for X-ray absorption experiments as described previously, and the same methods were used to protect these air-sensitive compounds from oxygen and water contamination.<sup>5</sup> The samples were loaded into a LHe-flow cryostat, and X-ray absorption measurements performed at the Stanford Synchrotron Radiation Lightsource on beamline 11-2. Data were collected at temperatures ranging from 30 to 300 K, using a Si(220) double-crystal monochromator. Fit methods were the same as described previously.<sup>5</sup> Reported spectra were energy calibrated by setting the first inflection point of the absorption spectrum on a Yb<sub>2</sub>O<sub>3</sub> reference sample to 8943 eV. Low temperature (ca. 2 K) EPR spectra were obtained with a Varian E-12 spectrometer equipped with an EIP-547 microwave frequency counter and a Varian E-500 gaussmeter, which was calibrated using 2,2-diphenyl-1-picrylhydrazyl (DPPH,  $g = 2.0036$ ).

**Calculations.** The ytterbium atom was treated with a small-core relativistic pseudopotential (RECP) ([Ar] + 3d)<sup>47</sup> in combination with its adapted basis set (segmented basis set that includes up to g functions). The carbon, nitrogen, oxygen, and hydrogen atoms were treated with an all-electron double- $\zeta$ , 6-31G(d,p).<sup>48</sup> All the calculations were carried out with the Gaussian 03 suite of programs<sup>49</sup> ORCA suite of program<sup>50</sup> either at the Density Functional Theory (DFT) level using the B3PW91<sup>51</sup> hybrid functional or at the CASSCF level; only one active space and inactive orbitals were used in the calculation. The geometry optimizations were performed without any symmetry constraints at either the DFT or the CASSCF level. The electrons were distributed over four 4f orbitals and the two  $\pi^*$  orbitals of phenanthroline.

**Syntheses.** The ligands, 1-10-phenanthroline (phen) and 4-methylphenanthroline (4-Mephen) were purchased from Aldrich while 5-methylphenanthroline (5-Mephen) was obtained from Tokyo Kasei Kokyo Co. All ligands were purified by sublimation between 80 and 200 °C/10<sup>-2</sup> mm prior to use. The ligands 3-methyl-1,10-phenanthroline (3-Mephen) and 3,8-dimethyl-1,10-phenanthroline (3,8-Me<sub>2</sub>phen) were synthesized according to a published procedure<sup>52</sup> and sublimed at 140 °C/10<sup>-2</sup> mmHg prior to use. <sup>1</sup>H NMR (3-Mephen): (CD<sub>3</sub>Cl, 295K, δ (ppm)) 9.18 (d, J = 7.8Hz, 1H), 9.03 (s, 1H), 8.23 (d, J = 7.8Hz, 1H), 8.02 (s, 1H), 7.74 (dd, J = 7.6, 3.2Hz, 1H), 7.74 (d, J = 7.2Hz, 1H), 7.61 (dd, J = 7.3, 3.2Hz, 1H), 2.61 (s, 3H). <sup>1</sup>H NMR (3,8-Me<sub>2</sub>phen): (CD<sub>3</sub>Cl, 296K, δ (ppm)) 9.05 (s, 2H), 8.64 (s, 2H), 7.74 (s, 2H), 2.64 (s, 6H).

**Cp<sup>\*</sup><sub>2</sub>Yb(phen) (1).** The complex Cp<sup>\*</sup><sub>2</sub>Yb(OEt<sub>2</sub>) (0.217 g, 0.420 mmol) was combined with 1,10-phenanthroline (0.095g, 0.420 mmol) and toluene (30 mL) was added at room temperature. The resulting purple/blue solution was stirred for 2h at room temperature as a dark powder formed. The suspension was cooled at -20°C and the dark colored powder was collected by filtration (125 mg, 83%). The dark powder was washed with toluene (3x5mL) and was heated in toluene (20 mL, 80°C), filtered while hot and slowly cooled at room temperature and then at -20°C. The dark microcrystalline purple powder was collected by filtration and dried under reduced pressure (70 mg, 47%). An alternative method was used in order to obtain crystals suitable for X-ray diffraction data collection by crystallization from toluene. A toluene solution of 1,10-phenanthroline (0.033 g, 0.186 mmol) was carefully layered at the top of a toluene solution of Cp<sup>\*</sup><sub>2</sub>Yb(OEt<sub>2</sub>) (0.096 g, 0.186 mmol). Slow diffusion of the two solutions overnight (16h) resulted in formation of X-Ray quality crystals at the interface and along the walls of the Schlenk flask that were collected by filtration and dried under reduced pressure (75 mg, 68%). M.p. 295-297°C (lit 297-300°C).<sup>14</sup> <sup>1</sup>H NMR: (toluene-d<sub>8</sub>, 299 K, δ (ppm)) 139.94 (2H, phen), 47.87 (2H, phen), 14.02 (2H, phen), 4.14

(30H, Cp<sup>\*</sup>), 0.47 (2H, phen). Crystals of Cp<sup>\*</sup><sub>2</sub>Yb(phen) are sparingly soluble in C<sub>7</sub>D<sub>8</sub> or THF-d<sub>8</sub>. The <sup>1</sup>H NMR spectrum was obtained from a warmed concentrated C<sub>7</sub>D<sub>8</sub> solution measured at 299 K. Anal. Calcd for C<sub>32</sub>H<sub>38</sub>N<sub>2</sub>Yb: C, 61.62; H, 6.14; N, 4.49. Found: C, 61.99; H, 6.04; N, 4.45. IR (cm<sup>-1</sup>): 1610 (m), 1590 (w), 1550 (w), 1498 (m), 1445 (s), 1359 (s), 1308 (s), 1290 (m), 1224 (w), 1172 (w), 1117 (m), 1054 (m), 1022 (w), 859 (w), 823 (m), 798 (m), 734 (m), 689 (m). Crushed crystals of Cp<sup>\*</sup><sub>2</sub>Yb(phen) sublimed in a 180 °C – 190 °C temperature range in an ampoule sealed under vacuum afforded crystals of Cp<sup>\*</sup><sub>2</sub>Yb(phen) (34 mg) over a one month period of time.

**[Cp<sup>\*</sup><sub>2</sub>Yb(phen)]<sup>+</sup>I<sup>-</sup> (2).**<sup>14</sup> The complex Cp<sup>\*</sup><sub>2</sub>Yb(OEt<sub>2</sub>) (0.172g, 0.333 mmol) was combined with 1,10-phenanthroline (0.060g, 0.333 mmol) and AgI (0.078g, 0.333 mmol). Toluene (40 mL) was added at room temperature and the purple solution was stirred for 16h at room temperature. The supernatant liquid was removed and the brown residue was extract with CH<sub>2</sub>Cl<sub>2</sub>. The solution was red and a grey residue remained. The solution was filtered, concentrated to 5 mL and cooled to -20°C. Large red crystals formed (120mg, 48%). mp: 175-180°C. <sup>1</sup>H NMR: (CD<sub>2</sub>Cl<sub>2</sub>, 300K, δ (ppm)) 280.87 (2H, phen) 52.43 (2H, phen), 9.52 (2H, phen), 5.31 (2H, CH<sub>2</sub>Cl<sub>2</sub>), 3.82 (30H, Me<sub>5</sub>C<sub>5</sub>), -2.48 (2H, phen). N.B. In a previous paper,<sup>14</sup> δ at 280 ppm was not observed and CHDCl<sub>2</sub> was assigned as a phen resonance. Anal. Calcd for C<sub>32</sub>H<sub>38</sub>N<sub>2</sub>YbI<sub>2</sub>•1.5CH<sub>2</sub>Cl<sub>2</sub>: C, 45.83; H, 4.71; N, 3.19. Found: C, 45.98; H, 4.50; N, 3.38. IR (cm<sup>-1</sup>): 1622 (w), 1518 (w), 1460 (s), 1415 (m), 1377 (s), 1273 (w), 855 (m), 728 (s).

**Cp<sup>\*</sup><sub>2</sub>Yb(3,8-Me<sub>2</sub>phen)•(C<sub>7</sub>H<sub>8</sub>) (3).** The complex Cp<sup>\*</sup><sub>2</sub>Yb(OEt<sub>2</sub>) (0.100 g, 0.192 mmol) was combined with 3,8-dimethyl-1,10-phenanthroline (3,8-Me<sub>2</sub>phen, 0.040 g, 0.192 mmol) and toluene (10mL) was added at room temperature. The deep purple solution was stirred for 2h at room temperature, concentrated to ca. 5mL, warmed to dissolve the dark residue and the resulting dark solution was filtered while warm. The filtrate was slowly cooled at -20°C. Dark purple-red crystals suitable for X-ray crystallography formed overnight. A second crop was

obtained. (Combined yield, 82 mg, 66%). mp: 286-288°C. Anal. Calcd for  $C_{34}H_{42}N_2Yb \cdot C_7H_8$ : C, 66.20; H, 6.77; N, 3.77. Found: C, 65.76; H, 6.65; N, 3.38. IR ( $cm^{-1}$ ): 1625 (w), 1573 (w), 1461 (s), 1410 (w), 1377 (s), 1261 (s), 1214 (w), 1153 (m), 1079 (s), 1020 (s), 861 (w), 799 (s), 728 (m), 692 (m).

**$Cp^*_2Yb(5-Mephen)$  (4).** The complex  $Cp^*_2Yb(OEt_2)$  (0.160 g, 0.309 mmol) was combined with 5-methyl-1,10-phenanthroline (5-Mephen, 0.060g, 0.309 mmol). Toluene (10 mL) was added at room temperature and the purple solution was stirred for 2h at room temperature. The volume of solvent was concentrated to 5 mL, then cooled at -20°C. A dark powder formed overnight which was crystallized from warm toluene (152 mg, 77%). NMR: (toluene- $d_8$ , 300K,  $\delta$  (ppm) 138.72 (1H, phen), 138.59 (1H, phen), 47.92 (1H, phen), 39.33 (1H, phen), 14.18 (1H, Phen), 11.40 (1H, phen), 4.09 (30H,  $C_5Me_5$ ), 0.06 (1H, phen), -0.58 (3H, Mephen). mp: 280-283°C. Anal. Calcd for  $C_{33}H_{40}N_2Yb$ : C, 62.15; H, 6.32; N, 4.39. Found: C, 61.74; H, 6.02; N, 4.32. IR ( $cm^{-1}$ ): 1626 (m), 1605 (w), 1578 (w), 1550 (w), 1504 (m), 1444 (s), 1377 (vw), 1355 (s), 1322 (s), 1281 (m), 1221 (vw), 1161 (m), 1136 (m), 1085 (vw), 1054 (m), 994 (w), 878 (m), 807 (w), 787 (w), 773 (m), 709 (w), 696 (m).

**$Cp^*_2Yb(4-Mephen)$  (5).** The complex  $Cp^*_2Yb(OEt_2)$  (0.304 g, 0.588 mmol) was dissolved in diethyl ether and added dropwise over 30 min to a cold diethyl ether suspension (10 mL, -77°C) of 4-methyl-1,10-phenanthroline (4-Mephen, 0.114 g, 0.588 mmol). While adding the phenanthroline, the suspension progressively turned to deep blue. When the addition was complete, the suspension was stirred at -77°C for 2 h and filtered to afford a dark blue-green powder (210 mg, 56%) which was washed with cold diethyl ether (2x10 mL, -77°C) and dried under reduce pressure.  $^1H$  NMR: ( $C_6D_6$ , 295K,  $\delta$  (ppm), 4.03 ( $Cp^*$ ), the only discernable peak. mp: 254-256°C. Anal. Calcd for  $C_{33}H_{40}N_2Yb$ : C, 62.15; H, 6.32; N, 4.39. Found: C, 62.06; H, 6.43; N, 4.55. IR ( $cm^{-1}$ ): 3069 (w), 3021 (w), 2954 (s), 2724 (w), 1634 (m), 1618 (m), 1512 (m), 1445 (s), 1401 (w), 1376 (w), 1354 (m), 1321 (w), 1301 (s), 1261 (w), 1190 (w), 1157



(w), 1086 (m), 1062 (w), 1048 (w), 1022 (w), 898 (s), 858 (m), 824 (m), 800 (s), 779 (w), 767 (w), 737 (w), 691 (w), 665 (w).

**Cp<sup>\*</sup><sub>2</sub>Yb(3-Mephen)·0.5(C<sub>7</sub>H<sub>8</sub>) (6).** The complex Cp<sup>\*</sup><sub>2</sub>Yb(OEt<sub>2</sub>) (0.105 g, 0.203 mmol) was combined with 3-methyl-1,10-phenanthroline (3-Mephen, 0.040 g, 0.203 mmol) and toluene (10mL) was added at room temperature. The deep purple solution was stirred for 2h at room temperature and a dark precipitate formed. The suspension was warmed to dissolve the dark powder and the resulting solution was filtered while warm. The filtrate was slowly cooled to -20°C to yield a dark microcrystalline powder. Two crop were obtained (Combined yield, 85 mg, 65%). <sup>1</sup>H NMR: (toluene-d<sub>8</sub>, 295K, δ (ppm) 121.47 (1H, phen), 118.38 (1H, phen), 59.15 (1H, phen), 57.17 (1H, phen), 55.02 (1H, Phen), 52.07 (1H, phen), 18.69 (1H, phen), 3.79 (30H, C<sub>5</sub>Me<sub>5</sub>), -9.51 (3H, Me-phen). mp: 270-272°C. Anal. Calcd for C<sub>33</sub>H<sub>40</sub>N<sub>2</sub>Yb·0.5(C<sub>7</sub>H<sub>8</sub>): C, 64.11; H, 6.49; N, 4.10. Found: C, 64.40; H, 6.49; N, 3.96. <sup>1</sup>H NMR spectrum confirmed the presence of the toluene. MS: {Cp<sup>\*</sup><sub>2</sub>Yb(3-Mephen)}, m/z = 638. IR (cm<sup>-1</sup>): 1612 (m), 1554 (w), 1494 (w), 1454 (s, nujol), 1377 (s), 1364 (s), 1320 (s), 1297 (s), 1229 (m), 1174 (m), 1118 (m), 1065 (m), 1022 (w), 886 (m), 880 (m), 776 (m), 731 (s), 696 (m), 675 (m).

**Cp<sup>\*</sup><sub>2</sub>Yb(5,6-Me<sub>2</sub>phen) (7).** The complex Cp<sup>\*</sup><sub>2</sub>Yb(OEt<sub>2</sub>) (0.208 g, 0.403 mmol) was combined with 5,6-dimethyl-1,10-phenanthroline (5,6-Me<sub>2</sub>phen, 0.0838 g, 0.403 mmol) and toluene (20 mL) was added at room temperature. The deep purple solution was stirred for 16 h at room temperature, concentrated to ca. 5 mL, warmed to dissolve the dark residue and filtered while hot. The filtrate was slowly cooled at -20 °C. A dark purple microcrystalline powder formed (204 mg, 78%) which was crystallized in warm cyclohexane yielding block-like purple X-ray suitable crystals (125mg, 48%). <sup>1</sup>H NMR: (toluene-d<sub>8</sub>, 300K) δ (ppm) 137.44 (2H, phen), 44.10 (2H, phen), 14.66 (2H), 3.95 (30H, C<sub>5</sub>Me<sub>5</sub>), 0.03 (6H, Me-phen). mp: 285-287°C. Anal. Calcd for Anal. Calcd. for C<sub>34</sub>H<sub>42</sub>N<sub>2</sub>Yb: C, 62.66; H, 6.50; N, 4.30. Found: C, 62.74; H, 6.43; N, 4.37. IR (cm<sup>-1</sup>): 1605 (m), 1584 (w), 1480 (w), 1426 (s), 1375 (m), 1345 (w), 1305 (w),

1275 (vw), 1218 (vw), 1190 (w), 1167 (w), 1145 (w), 1073 (w), 1019 (w), 943 (w), 804 (s), 758 (w), 736 (s), 686 (m). The crystal data, Table 10, for **7-crystallized** were obtained on crystals obtained by crystallization from cyclohexane. The crystal data, Table 10, for **7-sublimed**, were obtained on crystals that were crystallized from cyclohexane then sublimed in an ampoule sealed under vacuum at 195 °C over a period of two months. The sublimate contained needles and block-like crystals that were separated manually. The needles had the same unit cell parameters as those obtained for **7-crystallized**. The block-like crystals crystallized in the same crystal system and space group but with different cell parameters and contained only one molecule in the unit cell, Table 10.

#### Variable temperature <sup>1</sup>H NMR spectra of 3.

**Toluene-d<sub>8</sub>.** <sup>1</sup>H NMR: (toluene-d<sub>8</sub>, 300K) A major species, labeled S, was observed at δ (ppm) 95.54 (2H, phen), 51.07 (2H), 3.83 (2H, phen), 3.63 (30H, C<sub>5</sub>Me<sub>5</sub>), -10.02 (6H, Me-phen) and two minor species (labeled A<sub>1</sub> and A<sub>2</sub> accounting for less than 5% of the total) were observed. When the NMR tube was cooled, the two minor species observed at room temperature increased in intensity that represent two unsymmetrical (the position 2 and 9, 3 and 8, 4 and 7 and 5 and 6 are not equivalent) complexes in agreement with the formation of two isomeric dimers. The three different species are labeled S, for the symmetrical monomer, A<sub>1</sub> and A<sub>2</sub> for the two asymmetric isomeric dimers. In toluene, one proton could not be observed for A<sub>1</sub> and A<sub>2</sub>, presumably because it was under the toluene resonances. The amount of A<sub>1</sub> and A<sub>2</sub> is 40 % / 60 % at 210 K and this ratio is only slightly temperature dependent. <sup>1</sup>H NMR: (toluene-d<sub>8</sub>, 210K) δ (ppm) 105.21 (0.13H, phen-S), **89.95** (0.6H, Me-A<sub>1</sub>), **85.51** (1H, Me-A<sub>2</sub>), 74.24 (0.13H, phen-S), 56.20 (0.2H, phen-A<sub>1</sub>), 45.99 (0.33H, phen-A<sub>2</sub>), **22.66** (1H, Me-A<sub>2</sub>), 14.06 (0.50H, br, phen-A<sub>1</sub>+phen-A<sub>2</sub>), 4.41 (0.13H, phen-S), 3.63 (2H, Cp<sup>\*</sup>-S), -0.85 (16.5H, br, ν<sub>1/2</sub>=1100Hz, Cp<sup>\*</sup>-A<sub>1</sub>+A<sub>2</sub>), **-13.44** (0.6H, Me-A<sub>1</sub>), -15.42 (0.33H, phen-A<sub>2</sub>), -21.20 (0.2H, phen-A<sub>1</sub>), **-27.10** (0.4H, Me-S), -43.25 (0.2H, phen-A<sub>1</sub>), -70.24 (0.33H, phen-

A<sub>2</sub>), -111.47 (0.33H, phen-A<sub>2</sub>), -113.58 (0.2H, phen-A<sub>1</sub>). **THF-d<sub>8</sub>**. <sup>1</sup>H NMR: (thf-d<sub>8</sub>, 300K) δ (ppm) 72.72 (2H, phen), 42.33 (2H), 5.21 (2H, phen), 2.79 (30H, C<sub>5</sub>Me<sub>5</sub>), -7.01 (6H, Me-phen) and two minor species (less than 5% total). In THF, two protons could not be detected for each dimer (A<sub>1</sub> and A<sub>2</sub>). The amount of the isomers A<sub>1</sub> and A<sub>2</sub> is 55%-45% at 198K and is only slightly temperature dependant. <sup>1</sup>H NMR: (thf-d<sub>8</sub>, 198K) δ (ppm) **96.76** (1H, Me-A<sub>1</sub>), **92.01** (0.8H, Me-A<sub>2</sub>), 79.94 (0.27H, phen-S), 60.91 (0.22H, phen-A<sub>2</sub>), 60.04 (0.27H, phen-S), 49.99 (0.25H, phen-A<sub>1</sub>), **23.55** (0.8H, Me-A<sub>2</sub>), 13.03 (0.5H, br, phen-A<sub>1</sub>+phenA<sub>2</sub>), 5.70 (0.27H, phen-S), 2.91 (4.1H, Cp<sup>\*</sup>-S), -1.52 (18H, br, ν<sub>1/2</sub>=1200 Hz, Cp<sup>\*</sup>-A<sub>1</sub>+A<sub>2</sub>), **-15.09** (1H, Me-A<sub>1</sub>), -16.74 (0.25H, phen-A<sub>1</sub>), **-19.44** (0.8H, Me-S), -24.38 (0.22H, phen-A<sub>2</sub>), -42.09 (0.25H, phen-A<sub>1</sub>), -75.78 (0.22H, phen-A<sub>2</sub>).

Resonances in bold were the resonances used for the integration and the calculation of equilibrium constants. They were used because they are singlets whose resonances are clearly visible over the temperature range of the study (197.5 – 315 K). These calculations assume that the reaction shown in eq. 2, where M is the symmetric set, S, and D the asymmetric sets of resonances, A<sub>1</sub> and A<sub>2</sub>.

## X-Ray Crystallography.

**Table 10.** Selected Crystal Data and Data Collection Parameters for Cp<sup>\*</sup><sub>2</sub>Yb(phen) (**1**), crystallized and sublimed, and Cp<sup>\*</sup><sub>2</sub>Yb(3,8-Me<sub>2</sub>phen) C<sub>7</sub>H<sub>8</sub> (**3**), Cp<sup>\*</sup><sub>2</sub>Yb(5,6-Me<sub>2</sub>phen) (**7-crystallized**) and Cp<sup>\*</sup><sub>2</sub>Yb(5,6-Me<sub>2</sub>phen) (**7-sublimed**).

	[Cp <sup>*</sup> <sub>2</sub> Yb(phen)] <sub>2</sub> ( <b>1-dimer, crystallized</b> )	Cp <sup>*</sup> <sub>2</sub> Yb(phen) ( <b>1-monomer, sublimed</b> )	Cp <sup>*</sup> <sub>2</sub> Yb(3,8-Me <sub>2</sub> phen) · C <sub>7</sub> H <sub>8</sub> ( <b>3</b> )	Cp <sup>*</sup> <sub>2</sub> Yb(5,6-Me <sub>2</sub> phen) ( <b>7-crystallized</b> )	Cp <sup>*</sup> <sub>2</sub> Yb(5,6-Me <sub>2</sub> phen) ( <b>7-sublimed</b> )
Formula	C <sub>64</sub> H <sub>76</sub> N <sub>4</sub> Yb <sub>2</sub>	C <sub>32</sub> H <sub>38</sub> N <sub>2</sub> Yb	C <sub>41</sub> H <sub>50</sub> N <sub>2</sub> Yb	C <sub>34</sub> H <sub>48</sub> N <sub>2</sub> Yb	C <sub>34</sub> H <sub>48</sub> N <sub>2</sub> Yb
Crystal size (mm)	0.1 x 0.08 x 0.05	0.15 x 0.15 x 0.10	0.20 x 0.20 x 0.08	0.3 x 0.30 x 0.25	0.11 x 0.07 x 0.04
cryst system	Orthorhombic	Triclinic	Triclinic	Monoclinic	Monoclinic
space group	P b c a	P -1	P -1	P2(1)/n	P2(1)/n
volume (Å <sup>3</sup> )	V = 5221.3(7)	V = 1332.1(5)	V = 1710.3(4)	V = 8546(2)	V = 2883.48(17)
<i>a</i> (Å)	<i>a</i> = 17.9675(15)	<i>a</i> = 9.656(2)	<i>a</i> = 9.4244(13)	<i>a</i> = 9.7032(13)	<i>a</i> = 9.0108(3)
<i>b</i> (Å)	<i>b</i> = 17.8594(15)	<i>b</i> = 9.741(2)	<i>b</i> = 13.0969(18)	<i>b</i> = 31.081(4)	<i>b</i> = 17.2862(6)
<i>c</i> (Å)	<i>c</i> = 16.2715(13)	<i>c</i> = 14.998(4)	<i>c</i> = 14.5221(19)	<i>c</i> = 28.751(4)	<i>c</i> = 18.5122(6)
<i>α</i> (deg)	90.00	78.909(4)	83.002(2)	90	90
<i>β</i> (deg)	90.00	83.300(3)	77.287(2)	99.71	90.228(2)
<i>γ</i> (deg)	90.00	74.702(4)	78.976(2)	90	90
Z	4	2	2	12	4
formula weight (g/mol)	1237.36	623.68	743.87	651.74	651.74
density (calcd) (g cm <sup>-3</sup> )	1.587	1.555	1.444	1.520	1.501
absorption coefficient (mm <sup>-1</sup> )	3.605	3.533	2.755	3.308	3.268
F(000)	2512	628	660	3960	1320
temp (K)	100(1)	100(1)	100(1)	137(2)	100(1)
diffractometer <sup>a</sup>	SMART APEX	SMART APEX	SMART APEX	SMART 1000 CCD	APEX II QU/AZAR
θ range for data collection (deg)	2.04 to 26.61	1.39 to 25.43	1.44 to 25.35	2.44 to 25.46	1.61 to 25.44
transmission range	0.715 - 0.835	0.595 to 0.702	0.582 - 0.802	0.386 to 0.516	0.760 to 0.877
absorption correction	Multi-scan	Multi-scan	Multi-scan	multi scan	multi scan
total no. reflections	59465	26301	34871	102744	42405
unique reflections [R <sub>int</sub> ]	4179 [0.0690]	4882 [0.0352]	6213 [0.0514]	12833 [0.0710]	5333[0.0202]
final R <sup>b</sup> indices [I > 2σ(I)]	R = 0.0344, R <sub>w</sub> = 0.0783	R = 0.0305, R <sub>w</sub> = 0.0712	R = 0.0369, R <sub>w</sub> = 0.0844	R = 0.0369, R <sub>w</sub> = 0.0653	R = 0.0205, R <sub>w</sub> = 0.0463
R indices (all data)	R = 0.0563, R <sub>w</sub> = 0.0855	R = 0.0364, R <sub>w</sub> = 0.0739	R = 0.0448, R <sub>w</sub> = 0.0882	R = 0.0588, R <sub>w</sub> = 0.0676	R = 0.0239, R <sub>w</sub> = 0.0482
largest diff. peak and hole (e·Å <sup>-3</sup> )	1.20 and -0.799	0.859 and -1.067	1.235 and -1.252	1.225 and -0.917	0.605 and -0.393
GooF	1.003	1.178	1.070	0.980	1.074

<sup>a</sup> Radiation: graphite monochromated Mo Kα (λ = 0.71073 Å).

<sup>b</sup> R = Σ||F<sub>o</sub>| - |F<sub>c</sub>||/Σ|F<sub>o</sub>|.

Single crystals of the compounds **1-dimer**, crystallized and sublimed, and **3** were coated in Paratone-N oil and mounted on a Kaptan loop. The loop was transferred to a Bruker SMART APEX, diffractometer equipped with a CCD area detector.<sup>53</sup> Preliminary orientation matrixes and cell constants were determined by collection of 10 s frames for **3**, **7-crystallized** and **7-sublimed** and 20 s for **1-dimer** crystallized and 10 s for **1-monomer** sublimed, followed by spot integration and least-squares refinement. Data were integrated by the program SAINT<sup>54</sup> to a maximum  $2\theta$  value of  $50.94^\circ$  for **1-dimer**, crystallized,  $50.83^\circ$  for **1-monomer**, sublimed and  $50.70^\circ$  for **3**,  $50.48^\circ$  for **7-crystallized** and  $50.88^\circ$  for **7-sublimed**. The data were corrected for Lorentz and polarization effects. Data were analyzed for agreement and possible absorption using XPREP. A semi-empirical multi-scan absorption correction was applied using SADABS.<sup>55</sup> This models the absorption surface using a spherical harmonic series based on differences between equivalent data. The structures were solved by direct methods using SHELX<sup>56</sup> or SIR-97 and the WinGX program.<sup>57</sup> Non-hydrogen atoms were refined anisotropically and hydrogen atoms were placed in calculated positions and not refined for **3** and **1-dimer**, sublimed, **7-crystallized** but found in the Fourier map and refined isotropically for **7-sublimed**. For **1-dimer**, crystallized, only H28 was refined (The hydrogen located at the carbon atom where the coupling occurs). All the other were placed in calculated positions and not refined.

## ASSOCIATED CONTENT

**Supporting Information.** Information concerning magnetic susceptibility, Vis-NIR spectroscopy,  $^1\text{H}$  Variable Temperature NMR, X-ray crystallography; crystal data and CIF, CCDC 989736,  $[\text{Cp}^*_2\text{Yb}(\text{phen})]$ , CCDC 989737,  $[\text{Cp}^*_2\text{Yb}(\text{phen})]_2$ , CCDC 989938,  $[\text{Cp}^*_2\text{Yb}(3,8\text{-Me}_2\text{phen})]$ , CCDC 989939,  $[\text{Cp}^*_2\text{Yb}(5,6\text{-Me}_2\text{phen})]$ , sublimed and CCDC 989940,  $[\text{Cp}^*_2\text{Yb}(5,6\text{-Me}_2\text{phen})]$ , crystallized and calculated Cartesian coordinates for  $\text{Cp}_2\text{Yb}(\text{phen})$ ,  $\text{Cp}^*_2\text{Yb}(3,8\text{-Me}_2\text{phen})$ ,  $\text{Cp}^*_2\text{Yb}(5,6\text{-Me}_2\text{phen})$  and  $[\text{Cp}_2\text{Yb}(\text{phen})]_2$ .

## AUTHOR INFORMATION

\* **Corresponding Authors:** raandersen@lbl.gov, greg.nocton@polytechnique.edu

## ACKNOWLEDGMENT

G.N. would like to thank CNRS and Ecole polytechnique for funding. Work at University of California, Berkeley and at Lawrence Berkeley National Laboratory was supported by the Director, Office of Energy Research, Office of Basic Energy Sciences, Chemical Sciences Division, Heavy Element Chemistry Program of the U.S. Department of Energy under Contract No. DE-AC02-05CH11231. X-ray absorption data were collected at the Stanford Synchrotron Radiation Lightsource, a Directorate of SLAC National Accelerator Laboratory and an Office of Science User Facility operated for the U.S. Department of Energy Office of Science by Stanford University. We thank Antonio DiPasquale at CHEXRAY Berkeley for his help with crystal structures. L.M. is member of the Institut Universitaire de France. Cines and CALMIP are acknowledged for a generous grant of computing time. L.M. would also like to thank the Humboldt Foundation for a fellowship

## REFERENCES

- (1) *Inorg. Chem.* **2011**, *50*, issue 20, 9737-10516.
- (2) Booth, C. H.; Walter, M. D.; Daniel, M.; Lukens, W. W.; Andersen, R. A. *Phys. Rev. Let.* **2005**, *95*.
- (3) Walter, M. D.; Booth, C. H.; Lukens, W. W.; Andersen, R. A. *Organometallics* **2009**, *28*, 698.
- (4) Booth, C. H.; Kazhdan, D.; Werkema, E. L.; Walter, M. D.; Lukens, W. W.; Bauer, E. D.; Hu, Y.-J.; Maron, L.; Eisenstein, O.; Head-Gordon, M.; Andersen, R. A. *J. Am. Chem. Soc.* **2010**, *132*, 17537.
- (5) Booth, C. H.; Walter, M. D.; Kazhdan, D.; Hu, Y.-J.; Lukens, W. W.; Bauer, E. D.; Maron, L.; Eisenstein, O.; Andersen, R. A. *J. Am. Chem. Soc.* **2009**, *131*, 6480.
- (6) Da Re, R. E.; Kuehl, C. J.; Brown, M. G.; Rocha, R. C.; Bauer, E. D.; John, K. D.; Morris, D. E.; Shreve, A. P.; Sarrao, J. L. *Inorg. Chem.* **2003**, *42*, 5551.
- (7) Veauthier, J. M.; Schelter, E. J.; Carlson, C. N.; Scott, B. L.; Da Re, R. E.; Thompson, J. D.; Kiplinger, J. L.; Morris, D. E.; John, K. D. *Inorg. Chem.* **2008**, *47*, 5841.
- (8) Trifonov, A. A. *Eur. J. Inorg. Chem.* **2007**, 3151.
- (9) Trifonov, A. A.; Fedorova, E. A.; Fukin, G. K.; Druzhkov, N. O.; Bochkarev, M. N. *Ang. Chem. Int. Ed.* **2004**, *43*, 5045.
- (10) Trifonov, A. A.; Fedorova, E. A.; Ikorskii, V. N.; Dechert, S.; Schumann, H.; Bochkarev, M. N. *Eur. J. Inorg. Chem.* **2005**, 2812.
- (11) Lukens, W. W.; Magnani, N.; Booth, C. H. *Inorg. Chem.* **2012**, *51*, 10105.
- (12) Neumann, C. S.; Fulde, P. Z. *Phys B Condens. Matter* **1989**, *74*, 277.
- (13) Dolg, M.; Fulde, P.; Stoll, H.; Preuss, H.; Chang, A.; Pitzer, R. M. *Chem. Phys.* **1995**, *195*, 71.

- (14) Schultz, M.; Boncella, J. M.; Berg, D. J.; Tilley, T. D.; Andersen, R. A. *Organometallics* **2002**, *21*, 460.
- (15) Scarborough, C. C.; Wieghardt, K. *Inorg. Chem.* **2011**, *50*, 9773
- (16) McPherson, A. M.; Fieselmann, B. F.; Lichtenberger, D. L.; McPherson, G. L.; Stucky, G. D. *J. Am. Chem. Soc.* **1979**, *101*, 3425.
- (17) Gomberg, M. *Chem. Rev.* **1924**, *1*, 91.
- (18) McBride, J. M.; Vary, M. W. *Tetrahedron* **1982**, *38*, 765.
- (19) Neumann, W. P.; Uzick, W.; Zarkadis, A. K. *J. Am. Chem. Soc.* **1986**, *108*, 3762.
- (20) Small, D.; Rosokha, S. V.; Kochi, J. K.; Head-Gordon, M. *J. Phys. Chem. A* **2005**, *109*, 11261.
- (21) Zaitsev, V.; Rosokha, S. V.; Head-Gordon, M.; Kochi, J. K. *J. Org. Chem.* **2006**, *71*, 520.
- (22) Zheng, S. J.; Lan, J.; Khan, S. I.; Rubin, Y. *J. Am. Chem. Soc.* **2003**, *125*, 5786.
- (23) Wittman, J. M.; Hayoun, R.; Kaminsky, W.; Coggins, M. K.; Mayer, J. M. *J. Am. Chem. Soc.* **2013**, *135*, 12956.
- (24) Dugan, T. R.; Bill, E.; MacLeod, K. C.; Christian, G. J.; Cowley, R. E.; Brennessel, W. W.; Ye, S.; Neese, F.; Holland, P. L. *J. Am. Chem. Soc.* **2012**, *134*, 20352.
- (25) Suzuki, S.; Morita, Y.; Fukui, K.; Sato, K.; Shiomi, D.; Takui, T.; Nakasuji, K. *J. Am. Chem. Soc.* **2006**, *128*, 2530.
- (26) Fukui, K.; Sato, K.; Shiomi, D.; Takui, T.; Itoh, K.; Kubo, T.; Gotoh, K.; Yamamoto, K.; Nakasuji, K.; Naito, A. *Mol Cryst Liquid Cryst* **1999**, *334*, 49.
- (27) Goto, K.; Kubo, T.; Yamamoto, K.; Nakasuji, K.; Sato, K.; Shiomi, D.; Takui, T.; Kubota, M.; Kobayashi, T.; Yakusi, K.; Ouyang, J. Y. *J. Am. Chem. Soc.* **1999**, *121*, 1619.
- (28) Walter, M. D.; Berg, D. J.; Andersen, R. A. *Organometallics* **2006**, *25*, 3228.
- (29) Lukens, W. W.; Walter, M. D. *Inorg. Chem.* **2010**, *49*, 4458.
- (30) Camp, C.; Andrez, J.; Pécaut, J.; Mazzanti, M. *Inorg. Chem.* **2013**, *52*, 7078.
- (31) Camp, C.; Mougel, V.; Horeglad, P.; Pecaut, J.; Mazzanti, M. *J. Am. Chem. Soc.* **2010**, *132*, 17374.
- (32) Tilley, T. D.; Andersen, R. A.; Spencer, B.; Zalkin, A. *Inorg. Chem.* **1982**, *21*, 2647.
- (33) Ton, Q. C.; Bolte, M. *Acta Cryst.* **2005**, *E61*, 01406.
- (34) Rozenel, S. S. *Acta Cryst.* **2013**, *E69*, 01560.
- (35) Allen, F.; Kennard, O.; G., W. D.; L., B.; Orpen, A. G.; Taylor, R. *J. Chem. Soc. Perkin II* **1987**, S1.
- (36) Small, D.; Zaitsev, V.; Jung, Y. S.; Rosokha, S. V.; Head-Gordon, M.; Kochi, J. K. *J. Am. Chem. Soc.* **2004**, *126*, 13850.
- (37) Nocton, G.; Booth, C. H.; Maron, L.; Andersen, R. A. *Organometallics* **2013**, *32*, 1150.
- (38) Pali, A.; Tsukerblat, B.; Klokishner, S.; Dunbar, K. R.; Clemente-Juan, J. M.; Coronado, E. *Chem. Soc. Rev.* **2011**, *40*, 3130.
- (39) Pali, A.; Tsukerblat, B.; Modesto Clemente-Juan, J.; Coronado, E. *Int. Rev. Phys. Chem.* **2010**, *29*, 135.
- (40) Neidig, M. L.; Clark, D. L.; Martin, R. L. *Coord. Chem. Rev.* **2013**, *257*, 394.
- (41) Kaim, W. *J. Am. Chem. Soc.* **1982**, *104*, 3833.
- (42) Koizumi, T.; Yokoyama, Y.; Morihashi, K.; Nakayama, M.; Kikuchi, O. *Bull. Chem. Soc. Jpn.* **1992**, *65*, 2839.
- (43) Klein, A.; Kaim, W.; Waldhor, E.; Hausen, H. D. *J. Chem. Soc. Perkin II* **1995**, 2121.
- (44) Lauher, J. W.; Hoffmann, R. *J. Am. Chem. Soc.* **1976**, *98*, 1729.
- (45) Albright, T. A.; Burdett, J. K.; Whangbo, M.-H. *Orbital interactions in chemistry*; Wiley: Hoboken, New Jersey, 1985.
- (46) Walter, M. D.; Schultz, M.; Andersen, R. A. *New J. Chem.* **2006**, *30*, 238.
- (47) Dolg, M.; Stoll, H.; Preuss, H. *J. Chem. Phys.* **1989**, *90*, 1730.
- (48) Harihar, P.; Pople, J. A. *Theor. Chim. Acta* **1973**, *28*, 213.
- (49) Frisch, J.; Revision E-01 ed.; Gaussian Inc.: Pittsburgh, PA, 2001.
- (50) Neese, F.; Version 2.4. ed.; Chemie, M.-P.-I. f. B., Ed. Mülheim and der Ruhr, 2004.
- (51) Becke, A. D. *J. Chem. Phys.* **1993**, *98*, 5648.
- (52) Belser, P.; Bernhard, S.; Guerig, U. *Tetrahedron* **1996**, *52*, 2937.
- (54) Bruker Analytical X-Ray System, I. Madison, Winsconsin, USA, 2007.
- (55) Bruker Analytical X-Ray System, I. Madison, Winsconsin, USA, 2007.

- (55) Blessing, R. *Acta Cryst. A* **1995**, *51*, 33.
- (56) Sheldrick, G. *Acta Cryst. A* **2008**, *64*, 112.
- (57) Farrugia, L. *J. Appl. Crystallogr.* **1999**, *32*, 837.



## Table of Content

